Enhancing non-refractory aerosol apportionment from an urban industrial site through receptor modelling of complete high time-resolution aerosol mass spectra

M. L. McGuire[1], R. Y. –W. Chang[1,2]*, J. G. Slowik[1,2*], C. –H. Jeong[1], R. M. Healy[1], G. Lu[3], C. Mihele[3], J. P. D. Abbatt[1,2], J. R. Brook[3], G. J. Evans[1]

[1](Southern Ontario Centre for Atmospheric Aerosol Research, University of Toronto, 200 College St., Toronto, Ontario, Canada)

[2](Department of Chemistry, University of Toronto, St. George St., Toronto, Ontario, Canada)

[3](Air Quality and Research Division, Science and Technology Branch, Environment Canada, 4905 Dufferin St., Toronto, Ontario, Canada)

*Now at (School of Engineering and Applied Sciences and Department of Earth and Planetary Sciences, Harvard University, Cambridge, MA, United States)

*Now at (Paul Scherrer Institute, Laboratory of Atmospheric Chemistry, General Energy Research Department, Paul Scherrer Institute, Villigen, Switzerland, Villigen, Switzerland)

Correspondence to: G. J. Evans (greg.evans@utoronto.ca)

Abstract

Receptor modelling was performed on quadrupole unit mass resolution aerosol mass spectrometer (Q-AMS) sub-micron particulate matter (PM) chemical speciation measurements from Windsor, Ontario, an industrial city situated across the Detroit River from Detroit, Michigan. Aerosol and trace gas measurements were collected on board Environment Canada's CRUISER mobile laboratory. Positive matrix factorization (PMF) was performed on the AMS full particle-phase mass spectrum ($PMF_{Full\ MS}$) encompassing both organic and inorganic components. This approach was compared to the more common method of analysing only the organic mass spectra ($PMF_{Org\ MS}$). PMF of the full mass spectrum revealed that variability in the non-refractory sub-micron aerosol concentration and

composition was best explained by six factors: an amine-containing factor (Amine); an ammonium sulphate and oxygenated organic aerosol containing factor (Sulphate-OA); an ammonium nitrate and oxygenated organic aerosol containing factor (Nitrate-OA); an ammonium chloride containing factor (Chloride); a hydrocarbon-like organic aerosol (HOA) factor; and a moderately oxygenated organic aerosol factor (OOA). PMF of the organic mass spectrum revealed three factors of similar composition to some of those revealed through $PMF_{Full\ MS}$: Amine, HOA and OOA.

Including both the inorganic and organic mass proved to be a beneficial approach to analysing the unit mass resolution AMS data for several reasons. First, it provided a method for potentially calculating more accurate sub-micron PM mass concentrations, particularly when unusual factors are present, in this case, an Amine factor. As this method does not rely on a priori knowledge of chemical species, it circumvents the need for any adjustments to the traditional AMS species fragmentation patterns to account for atypical species, and can thus lead to more complete factor profiles. It is expected that this method would be even more useful for HR-ToF-AMS data, due to the ability to better understand the chemical nature of atypical factors from high resolution mass spectra. Second, utilizing PMF to extract factors containing inorganic species allowed for the determination of extent of neutralization, which could have implications for aerosol parameterization. Third, subtler differences in organic aerosol components were resolved through the incorporation of inorganic mass into the PMF matrix. The additional temporal features provided by the inorganic aerosol components allowed for the resolution of more types of oxygenated organic aerosol than could be reliably resolved from PMF of organics alone. Comparison of findings from the $PMF_{Full\ MS}$ and $PMF_{Org\ MS}$ methods showed that for the Windsor airshed, the $PMF_{Full\ MS}$ method enabled additional conclusions to be drawn in terms of aerosol sources and chemical processes. While performing $PMF_{Org\ MS}$ can provide important distinctions between types of organic aerosol, it is shown that including inorganic species in the PMF analysis can permit further apportionment of organics for unit mass resolution AMS mass spectra.

1 Introduction

Atmospheric aerosol or particulate matter (PM) is known to have important implications on atmospheric visibility (Watson, 2002), climate change (IPCC, 2013), and human health (Pope and Dockery, 2006; Anderson et al., 2012; Brook et al., 2010). Understanding the sources and processes responsible for PM composition and concentration is critical to enacting effective PM reduction strategies. Receptor modeling of PM chemical speciation data is one method towards achieving this. Historically, receptor modeling studies have focused on understanding integrated filter measurements, which have been particularly useful for providing an overview of the main chemical components of major source categories, and their longer-term temporal trends (Gordon, 1980; Hopke, 2003; Watson et al., 2008). More recently, receptor modeling analyses have been focused on online high time-resolution chemical analysis techniques, as they can provide additional insight on sources and processes not captured by the chemical or temporal resolution of daily filter measurements.

Aerosol mass spectrometry is among the most widely used high-time resolution PM chemical speciation methods that can be used to quantify the impacts of non-refractory source components, including both organic and inorganic components. Receptor modeling, namely Positive Matrix Factorization (PMF), has become a useful analytical technique to further understand the origins of AMS measured aerosol. Among these studies, most have focused on the organic fraction of the AMS mass spectrum (e.g., Lanz et al., 2007; Ulbrich et al., 2009) in an effort to resolve uncertainty regarding the sources and processes contributing to secondary organic aerosol (SOA), an aerosol component with potential implications on climate (IPCC, 2013). Many of these studies have focused on the application of factor analysis to the organic mass fraction in an attempt to deconvolve it into descriptive sub-components, namely a hydrocarbon-like organic aerosol (HOA) factor, and an oxygenated organic aerosol (OOA) factor. Examination of datasets from numerous, diverse environments has shown that the OOA fraction often splits into two sub-components, OOAI and OOAII (Zhang et al., 2011). Observations of their temporal behavior have shown that these two factors typically exhibit different volatility regimes, whereby OOAII exhibits significant diurnal variability associated with condensation and volatilization from temperature cycling. By contrast, OOAI has been mainly associated with synoptic flow regimes, with no significant association with temperature cycling. The semi-volatile OOAII type factor was first reported in a study by (Lanz et al., 2007), although its volatile nature was first substantiated with external measurements in a study by Huffman et al. (2009); in this study it was shown that decreased volatility of OA factors was associated with increasing oxygenation, or oxygen to carbon (O/C) ratio (Huffman et al., 2009). As a result, the OOAI and OOAII factors are often referred to in the literature as low-volatility OOA (LV-OOA), and semi-volatile OOA (SV-OOA) respectively (Jimenez et al., 2009). While the HOA and OOA components have been the most widely observed organic components deconvolved in the multitude of AMS studies performed to date (Zhang et al., 2007), other factors have been identified, such as biomass burning organic aerosol (BBOA) (e.g., Aiken et al., 2009), amine-containing organic aerosol (e.g., Aiken et al., 2009; Sun et al., 2012; Docherty et al., 2011; Hildebrandt et al., 2011) and even cooking organic aerosol (COA) (e.g., Lanz et al., 2007; Allan et al., 2010; Sun et al., 2011; Mohr et al., 2012; Crippa et al., 2013a). In many studies, correlation analysis of organics with inorganic species has been used to further ascertain the sources and processes contributing to a particular factor. For instance, significant correlations have been found between OOAI and SO_4^{2-}, and between OOAII and NO_3^- (Lanz et al., 2007; Ulbrich et al., 2008).

This study presents a receptor modeling analysis of high time-resolution unit mass resolution quadrupole AMS measurements. Aerosol and trace gas speciation measurements were made onboard Environment Canada's CRUISER (Canadian Regional and Urban Investigation System for Mobile Research) mobile laboratory at MicMac Park in Windsor, Ontario in the winter of 2005. A different approach was taken in this study with respect to the majority of previous receptor modeling analyses of the non-refractory sub-micron chemical composition, as PMF was applied to the full mass spectrum, comprising both the organic and inorganic components. To the authors' knowledge, combined PMF analysis of organic and inorganic AMS mass spectra has been performed in only three other studies (Chang et al., 2011; Sun et al., 2012; Crippa et al., 2013b). Of these, the study by Sun et al. was the only one to include all inorganic and organic species together. While PMF had previously been applied to data including AMS derived bulk concentrations of inorganic and organic species (e.g., Buset et al., 2006; Crippa et al., 2013b), Chang et al. were the first to apply the PMF multivariate deconvolution algorithm to combined organic and inorganic mass spectra, in that case to ambient arctic aerosol (Chang et al., 2011). However, low ambient aerosol concentrations, and low associated signal to noise ratios, prevented the inclusion of all species in the analysis. As a result, NH_4^+ was excluded, which precluded certain conclusions regarding aerosol neutralization from being drawn. Nonetheless, four factors were extracted in that study, including factors representing marine biogenic emissions (containing methanesulphonic acid or MSA), continental emissions, ship emissions, and OOA. Each factor was characterized by differing degrees of cross-apportionment between organic and inorganic species. Eight factors were identified in the study by Sun et al., many more than found in the Arctic study, mainly due to the urban sampling location in New York City (Sun et al., 2012). Similar to Chang et al., significant organic and inorganic cross-apportionment was noted for most of the factors. In the study by Crippa et al., only SO_4^{2-} related ions were included in the PMF analysis in addition to organics, which allowed for the apportionment of SO_4^{2-} ions to marine and terrestrial aerosol factors (Crippa et al., 2013b).

This study focuses on the physical interpretation of cross-apportionment between organic and inorganic non-refractory sub-micron PM species between factors. Drawing upon cold condition measurements from a complex, industrialized site, this analysis illustrates how this methodology can help to better understand underlying aerosol sources, and processes, and identify new scientific and methodological conclusions.

2 Experimental Methods

2.1 Aerosol mass spectrometer measurements

Aerosol and trace gas measurements were collected on board Environment Canada's CRUISER mobile laboratory, which was stationed at MicMac Park in Windsor (42°17'5.38"N, 83° 4'31.42"W) in January and early February 2005. Located next to Detroit on the Canada-US border in south-western Ontario, Windsor has historically been known experienced frequent episodes of poor air quality. Local sources of PM are numerous and diverse due to a large manufacturing base, including sources such as steelmaking, salt and gypsum mining, petrochemical refining, and coal-fired power generation. Another significant local source is traffic, given that the Windsor-Detroit border crossing is the largest international border crossing between Canada and the US. Regionally, Windsor is impacted by many sources, but perhaps most significantly by coal-fired power plants to the south in the Ohio River valley. A map of the Windsor/Detroit area is shown in Figure 1.

Chemical speciation measurements of submicron PM were made on board CRUISER using a unit mass resolution quadrupole aerosol mass spectrometer (Q-AMS) (Aerodyne Research Inc., Billerica, MA, USA). The AMS sampled from 12 January – 2 February 2005, except for a period of three days between 15 – 18 January when it was not operating. Sampling occurred at a 15min time resolution, except for a short period at the beginning of the campaign (12 to 13 January), when it sampled at a 5min time resolution. CRUISER samples air at 4m above ground level through a $PM_{2.5}$ sharp cut cyclone (Rupprecht and Patashnick, East Greenbush, NY, USA) at a flow rate of 16.7 litres per min (lpm), to supply a primary sampling line from which several on board PM and gas instruments are connected. The temperature in the sampling enclosure in wintertime is approximately 20°C, although sheath air surrounding the primary 1.25” diameter stainless steel sampling line maintains it at near ambient temperature. The AMS is connected to CRUISER’s primary sampling line by 0.8m of conductive tubing, and samples at a flow rate of 1 lpm. Although the aerosol was not dried prior to AMS sampling, the relative humidity (RH) remained close to that of the ambient air due to the use of sheath air, and relatively short sampling line. Filtered AMS measurements were performed at several times during the campaign, and were removed from the dataset, resulting in 1745 observations. The operating principles of the AMS instrument have been documented elsewhere (Jayne et al., 2000; Canagaratna et al., 2007b), although those of the Q-AMS are briefly outlined here. Particles are sampled through the particle inlet and focused into a collimated beam using an aerodynamic lens. The stream of particles impact a porous tungsten surface heated to ~600°C, whereupon the non-refractory components of the particles flash vaporize. The resulting gases are ionized by electron impact (EI, 70 eV), and the resulting ions are measured using a quadrupole mass spectrometer.

The AMS was calibrated for ionization efficiency by atomizing a NH_4NO_3 solution and then size-selecting 300nm particles using a TSI 3071 electrostatic classifier. A relative ionization efficiency (vs. NO_3^+) of 4.5 for NH_4^+ was required to obtain ion balance for the bulk NH_4NO_3 calibration particles, and this value was applied to the ambient data. Default relative ionization efficiencies were assumed for organics (1.4), chloride (1.3), nitrate (1.1), and sulphate (1.2).

The collection efficiency of the AMS is often estimated by comparison of the measured mass with that of a collocated instrument. If collocated external PM_1 mass measurements are unavailable, CE is often assumed by comparison of the combined AMS sub-micron PM mass and BC with an external measure of $PM_{2.5}$. Middlebrook et al., have also shown that a composition dependent CE can be estimated from the bulk aerosol composition (Middlebrook et al., 2012). These two options were investigated to determine whether a CE other than a default of 1 could be applied to the data, and the results of this investigation are presented in the Supplement. Ultimately, this analysis did not yield a reliable estimate of CE; as such no correction was applied to these data, and a default, simple integer collection efficiency of unity was assumed for this campaign. This value has been used in other studies (Lanz et al., 2007; Richard et al., 2011; Chirico et al., 2011), and reflects a lower bound for the non-refractory mass concentration. While an accurate estimate of collection efficiency is required for overall mass determination, it remains an integer value (either constant, or composition dependent) applied to the total mass concentration, and ultimately does not affect the primary study conclusions with respect to identifying and characterizing factors.

The time series of collected AMS mass spectra were separated into chemically resolved mass spectra (NH_4^+, NO_3^-, SO_4^{2-}, Cl^-, and organics) using pre-defined fragmentation patterns (Allan et al., 2004), as implemented in the Q-AMS analysis software Deluxe v1.43 for the IGOR Pro software package (Wavemetrics, Inc.).

2.2 Positive matrix factorization

Positive matrix factorization or PMF, (Paatero and Tapper, 1993, 1994; Paatero, 1997) is a non-negative factor analysis model that can be used to represent a time series of measurements as a linear combination of static factor profiles (ideally corresponding to specific sources and/or processes) and their time-dependent intensities. It is applied to an n x m matrix of data, X, and solves the general receptor equation:

$$x_{ij} = \sum_{k=1}^{p} g_{ik} f_{kj} + e_{ij} \quad , \qquad (1)$$

where n is the number of samples and m is the number of species; x_{ij} is the concentration of the j^{th} species in the i^{th} sample; g_{ik} is the contribution of the k^{th} factor to the i^{th} sample; f_{kj} is the mass fraction of the j^{th} species contributing to the k^{th} factor; e_{ij} is the residual concentration of the j^{th} species in the i^{th} sample; and p is the number of independent factors as chosen by the user. The general receptor equation is solved iteratively, using a Gauss-Newton, weighted least-squares algorithm, until the object function Q, is minimized:

$$Q = \sum_{i=1}^{n} \sum_{j=1}^{m} \left(\frac{e_{ij}}{s_{ij}} \right)^2 \qquad (2)$$

where s_{ij} is an element in the n x m matrix, S, of uncertainties corresponding to x_{ij}. The expected Q value is defined as:

$$Q_{expected} = nm - p(n+m) \qquad (3)$$

PMF analysis was performed using EPA PMF 4.1 (Norris et al., 2010). Two different approaches were taken in this study. One approach involved application of PMF to the organic mass spectra only ($PMF_{Org\ MS}$), and the other involved application of PMF to the full mass spectra ($PMF_{Full\ MS}$). As such, two different methodologies were required for data pre-treatment, and formulation of the data and error matrices.

The data and error matrices for the $PMF_{Org\ MS}$ analysis were prepared following principles outlined in Ulbrich et al. (2009). A total of 167 *m/z*'s were included in the PMF_{OrgMS} analysis (*m/z* 12 – 200), with *m/z*s excluded due to either low signal (e.g., 19-23), signal dominated by inorganic (e.g., 14) or gaseous (e.g., 28) species, or high background levels (e.g., 149) (Ulbrich et al., 2009; Zhang et al., 2005). Uncertainties for the $PMF_{Org\ MS}$ analysis were calculated according to the method of Allan et al. (2003), and a minimum error corresponding to the counting of a single ion was enforced throughout the dataset (Ulbrich et al., 2009). Within the AMS organic fraction extraction process, certain *m/z* (16, 17, 18, and 44) are assumed to be a constant fraction of *m/z* 44. The uncertainties of these ions were accordingly multiplied by sqrt(4) to prevent them from being over weighted by the PMF algorithm. The signal to noise ratio (S/N) for each *m/z* was calculated to identify weak (0.2 < S/N < 2), and bad (S/N < 0.2) variables; a downweighting policy was applied such that weak variables are downweighted by a factor of two, and bad variables excluded. No variables were designated as bad for this analysis.

The data and error matrices for the $PMF_{Full\ MS}$ analysis were prepared following principles outlined by Chang et al. (2011). The data matrix was calculated in nitrate equivalent (NO_{3eq}) mass (refer to section 2.3) and calculated by taking the entire raw MS matrix ("All"), and from it, subtracting the mass spectral matrices of species not of interest to the analysis (i.e., air and water), leaving the contributions from fragments associated with NH_4^+, NO_3^-, SO_4^{2-}, Cl^-, and organics. Downweighting of selective organic or inorganic peaks as is required when conducting the $PMF_{Org\ MS}$ analysis was avoided in the $PMF_{Full\ MS}$ analysis, as the $PMF_{Full\ MS}$ matrix resulted from the subtraction of the "Air" and "Water" components from the original "All" matrix. In other words, the $PMF_{Full\ MS}$ matrix was not constructed from application of the fragmentation scheme to create "Org", "SO_4^{2-}", "NO_3^-", "Chl", and "NH_4^+" matrices which could be added together to generate a "Full MS" matrix, but was a result of the subtraction of the "Air" and "Water" components subtracted from the original "All" matrix. The corresponding error matrix (in NO_{3eq} mass) was then constructed by adding in quadrature the "All_err", "Water_err", and "Air_err" matrices. Similar to the organic matrix preparation, a minimum uncertainty corresponding to a single ion was enforced, and the same S/N policy was applied, although no variables were designated as bad (Ulbrich et al., 2009). A total of

173 *m/z*s were included in the $PMF_{Full\ MS}$ analysis, with *m/z*s excluded due to either low signal (e.g., 19-23), known interferences (e.g., 18), signal dominated by gaseous species (e.g., 28), high background levels (e.g., 149), or non-linear contributions (*m/z* 39). While *m/z* 39 (potassium) could be useful in a PMF analysis of the full mass spectrum for the potential identification of certain factors (e.g., biomass burning), it was excluded due to non-linearities in the signal. Potassium can ionize by two different ionization pathways, namely electron impact and surface ionization, each bearing a different relative ionization efficiency (RIE) (Drewnick et al., 2006). Thus, the amount of signal measured from potassium depends not only on the actual initial potassium mass, but also the particle's history within the AMS. Quantifying the relative degree of vaporization via electron impaction vs. surface ionization is difficult, as this ratio is not entirely stable over time (e.g., minor drifts in tuning, fluctuations of the vaporizer temperature), and may depend on the particle composition. Initial PMF tests indicated that potassium inclusion did not aid in the extraction of a biomass burning organic aerosol factor. Although some potassium is also found at *m/z* 41, this fragment was dominated by organics (potassium contribution <7%). This signal could be removed, although doing so requires referring to non-linear *m/z* 39. Thus, due to the low contribution of potassium at *m/z* 41, this fragment was left unaltered to avoid introducing additional noise to the matrix.

In addition to the uncertainties as described above, a global uncertainty of 5% of the data (the C3 parameter) was added to the uncertainty matrix, in a similar fashion to (Brown et al., 2012). Solutions were interpreted based on the resulting factor profiles and temporal trends. The factor profile mass spectra were compared with those extracted from other PMF studies of AMS data, however it should be noted that these comparisons were interpreted with care due to methodological differences between $PMF_{Full\ MS}$ and $PMF_{Org\ MS}$ analyses. Factor temporal trends were examined for particular behaviors such as diurnal trends, and correlations with meteorological conditions and external species (e.g., gases and PM mass).

Two methods were employed to test the robustness of the factor analysis of the AMS data: FPeak rotational analysis and bootstrapping. The effect of global matrix rotations through the FPeak parameter was mainly evaluated in terms of the mass spectra: changes in the mass spectra could be more objectively evaluated than changes in temporal trends due to the availability of comparison mass spectra from other studies, and lack of a priori knowledge on source temporal trends. However, the effect of FPeak rotations on correlations between some factors and key external measurements was also evaluated. It should be noted that since EPA PMF 4.1 utilizes the multilinear engine (ME-2), FPeak values approximately five times greater than those typically used for PMF2 in order to achieve a similar degree of rotation (i.e., in PMF2, FPeaks explored typically range from -2 to 2) (Norris et al., 2010). Similar to the approach used by Brown et al. (2012), FPeak rotations were calculated from -10 to 10 in increments of 2 (Brown et al., 2012). This range led to increases in Q/Q_{exp} of ~1%, indicating that the base solution appeared rotationally unique. Furthermore, this rotational range appeared sufficient to provide indication of the relative robustness of factors, by comparing the relative degree of rotational ambiguity between factors: the robustness of each factor was examined by applying the AMS fragmentation species extraction algorithm (Allan et al., 2003) to the resulting FPeak factor profiles, and the species mass fractions across FPeak values was examined. In terms of the bootstrap analysis, 100 bootstrap iterations were performed. Bootstrap results were mainly interpreted according to the number of unmapped factors (factors which could not be "mapped" to the base case using a threshold uncentered correlation coefficient of 0.6). The results of these tests are described in the supplementary material.

2.3 Aerosol mass spectrometer mass quantification

The use of NO_{3eq} mass proved to be a useful method for obtaining better mass estimates, as the various relative ionization efficiencies (RIEs) of component species can be considered in the mass quantification of resolved PMF factors. In the case of PMF of organic MS, only a single multiplicative factor of is applied to the dataset as a whole to account for the RIE of organics (RIE of 1.4). However, another approach is required for mass estimates of multi-component, combined inorganic and organic mass spectra. Firstly, PMF analysis of the full mass spectrum was performed using nitrate equivalent mass (NO_{3eq}), whereby instrument signal was converted to mass using a single RIE (in this case, that for nitrate). Following PMF, the factor species composition was determined through application of the fragmentation to factor mass spectra (Allan et al., 2004;Allan et al., 2003), and an effective factor RIE calculated through weighted average of RIEs according to the factor composition (Chang et al., 2011). Default RIE values were assumed for the main AMS species, and used to convert the NO_{3eq} factor mass to "real" mass. It should be noted that this method works well when the defining species chemical nature is well understood, and fragmentation patterns and RIE values are available (i.e., as for NO_3^-, SO_4^{2-}, NH_4^+, chloride, organics). However, the AMS has been known to detect other species, such as methanesulphonic acid (Chang et al., 2011; Langley et al., 2010; Zorn et al., 2008), and amines (Silva et al., 2008;Docherty et al., 2011; Hildebrandt, et al., 2011), for which less information is available. In particular, it has been shown that depending on their chemical nature, amines may display a wide range of fragmentation patterns and RIE values (i.e., from 1.3 to 10) (Silva et al., 2008). Thus, an indication of the chemical nature of the factor species may be integral to the factor mass quantification calculation. Further discussion of the implication of these assumptions is provided in section 3.2.

2.4 Supporting measurements

Trace gases were measured using a variety of techniques, namely by quadrupole Proton Transfer Reaction Mass Spectrometry (PTR-MS) (Ionicon, Innsbruck, Austria) to measure VOC's, as well as other gas analyzers to measure NO_x, SO_2, O_3 and CO. Particle number concentration measurements were provided by a condensation particle counter (model 3010, TSI Inc., Shoreview, MN, USA). Black carbon measurements were also available from an aethalometer (Magee Scientific), and measurements derived from absorption at 880nm were used. As reliable collocated sub-micron PM mass concentration measurements were unavailable, PM mass comparisons were made to 5min $PM_{2.5}$ measurements obtained by a TEOM (TEOM model 1400ab, Rupprecht and Patashnick, East Greenbush, NY, USA) onboard CRUISER. Hourly meteorological measurements were supplied courtesy of Environment Canada, from a meteorological station located 10km to the east of MicMac Park in an open field at Windsor Airport (42°16'48"N, 82°57'36"W). Measurements of wind direction and speed, RH, and visibility were used in this analysis.

2.5 Assessment of geographic origins

The geographic origins of the AMS PMF factors were assessed using the conditional probability function (CPF), and the potential source contribution function (PSCF), which have been described elsewhere (McGuire et al., 2011; Ashbaugh et al., 1985). In this study, the CPF threshold was set to the top 25^{th} percentile, and probabilities associated with infrequently observed wind directions (winds < 5% of the time), were downweighted by 3. For the PSCF analysis, each cell was chosen to be 0.5° in both latitude and longitude, and the threshold for the PSCF was set to the top 50^{th} percentile. For the purposes of the Sulphate-OA factor PSCF analysis, three short events known to be associated with local sources were removed from the analysis (see section 3.1.2 for further description). The result is a probability distribution map where higher probabilities indicate more probable regional source regions.

3 Results and discussion

An overview of the meteorological conditions observed during the campaign is presented in Figure 2. Unusually warm January temperatures for southwestern Ontario were observed at the beginning of the campaign. Higher wind speeds were associated with southerly air flow. Wind speeds dropped dramatically towards the end of the campaign resulting in a stagnation period, resulting in a significant increase in PM mass concentration. The time series of the AMS non-refractory species, as calculated from the AMS data analysis package, is shown in Figure 3, and descriptive statistics for these species are listed in Table 1. On average, prior to PMF analysis, organic aerosol (37%), and NO_3^- (31%) were found to contribute most to the non-refractory sub-micron PM mass. The following sections first outline results from PMF analysis of the full mass spectrum, followed by PMF analysis of the organics. Finally, results from both analyses are compared.

3.1 PMF of AMS full mass spectra

$PMF_{Full\ MS}$ analysis showed that six factors best captured the variability in the data. The following factors were retrieved: Amine; Sulphate-OA, containing mostly ammonium sulphate; Nitrate-OA, containing mostly ammonium nitrate; Chloride, composed mostly of ammonium chloride; HOA, a hydrocarbon-like organic factor, which represented primary organic aerosol; and OOA, an oxygenated organic aerosol factor. Figures 4 and 5 show the time series (in local time) and factor profiles respectively. Figure 6 shows the mass spectra of each factor's organic components, and Figure 7 details each factor's chemical composition by species and factor component.

Solutions containing two through ten factors were analyzed. In brief, as with the six factor solution, the five, seven, and eight factor solutions contained almost the same five factors (Sulphate-OA, Nitrate-OA, Chloride, HOA, Amine). While the five factor solution did not extract an OOA factor, the seven factor solution split the OOA resolved from the six factor solution into a similar OOA factor, as well as an Other OA factor which did not sufficiently resemble any known mass spectra. The eight factor solution added a Local Sulphate factor. More detailed solution descriptions and justification of the six to eight factor solutions are presented in the supplement. The six factor solution was chosen because: among 100 random runs, all runs converged and displayed a constant, global minimum Q value; higher order solutions did not explain significantly more variance in the data; and factors from this solution were the most physically meaningful. The following sections detail findings for each factor with a focus on new insights into aerosol sources and processes due to the incorporation of both the organic and inorganic aerosol fractions into the PMF analysis.

3.1.1 Amine factor

The Amine factor's time series, shown in Figure 4, was characterized by several short duration events. The Amine factor MS (Figure 5) was distinctly different from the other factors due to the presence of fragments such as *m/z* 30, 58, 86, and 100. This factor also contained significant signal at *m/z* 30, with the *m/z* 30/46 ratio much higher than that for nitrate, suggesting the presence of other ions (e.g., CH_4N^+). The organic functionality of this factor was examined through the delta (Δ) pattern displayed by its mass spectral profile, whereby $\Delta = m/z - 14n + 1$ (where n is the number of CH_2 groups left on the functional group) (McLafferty and Tureček, 1993). Given its characteristic fragments, and strong $\Delta = 3$ pattern (i.e., 30, 44, 58, 72, 86, 100, etc.) representative of alkyl amines ($C_nH_{2n+2}N$), this factor was assigned as Amine. The Amine factor was robust in the solution, emerging in each solution involving at least three factors. In terms of assessing rotational ambiguity from FPeak analysis, the Amine factor appeared robust, and rotationally fixed (Figure 5).

Gas and particle phase amines have been recorded in the troposphere for some time, and can be emitted from a variety of sources. The largest global sources of amines are animal husbandry, industrial operations, and waste-water treatment (Ge et al., 2011). Gaseous aliphatic amines at high concentrations can have serious consequences for human health, with effects ranging from irritation of mucosal membranes, to blood clots, and potentially cancer (Greim et al., 1998). Particle-phase amines have been measured in widely different settings, ranging from rural areas in Utah (Silva et al., 2008) and Ontario (McGuire et al., 2011; Rehbein et al., 2011), to heavily urbanized areas, such as Mexico city (Aiken et al., 2009), Riverside, California (Pratt et al., 2009), and Toronto (Tan et al., 2002; Rehbein et al., 2011). In this study, the measurement site was located in an urban industrial setting, with known amine sources located nearby: a waste-water reclamation plant, and a major amine chemical manufacturer were located 1 and 13km to the southwest, respectively. According to the TRI and NPRI inventories, the amine manufacturer was the largest monitored emitter of TEA in 2005 in the Windsor/Detroit region (US EPA, 2013; Environment Canada, 2013). The strong southwest directionality observed in the CPF (Figure 8a) indicated that both of these sources may have contributed. The sharp bursts in temporality were consistent with local sources, such as fugitive emissions from industrial operations.

In order to quantify the Amine factor's mass concentration, it was necessary to obtain an estimate of the factor's effective RIE. Unfortunately, an effective RIE could not be determined through application of the traditional AMS fragmentation table, as the factor contained amines that were not represented in the table. It is possible to alter the fragmentation table to include additional species, provided the nature of the measured species is known, and a species fragmentation pattern is available. This has as has previously been accomplished, for instance, with methanesulphonic acid (MSA) (Chang et al., 2011; Langley et al., 2010; Zorn et al., 2008). In a study by Chang et al., MSA could be positively identified due to unique marker fragments and a lack of interfering species, and its mass could be calculated through application of a laboratory determined fragmentation pattern and RIE (Chang et al., 2011). Taking this approach was not obvious for the present study, as the particular amine compound(s) could not be easily identified, and there was a possibility that the factor represented a linear combination of different amine species with different RIEs and fragmentation patterns.

Nonetheless, the nature of the Amine factor was investigated to determine a potential factor RIE for mass estimation. Amines have been shown to exhibit a wide range of RIEs, depending on their chemical nature. AMS measurements of amines present in salt form, such as methylammonium chloride, dimethylammonium chloride, and trimethylammonium chloride, have shown that the amine fraction in these compounds can display RIEs from 5 to 10 (Silva et al., 2008). However, oxidized alkyl amines such as trimethylamine-n-oxide (TMAO) have been shown to ionize with an RIE of 1.3, a value closer to organics (RIE = 1.4) (Silva et al., 2008). It has been hypothesized that aminium salts exhibit a relatively high RIE due to surface ionization on the AMS vaporizer, similar to that observed for potassium salts (Silva et al., 2008). Thus, depending on the type of amine compound or mixture of compounds the Amine factor represents, its RIE may lie within a wide range (i.e., 1.3 – 10).

A reasonable estimate for an effective RIE for the Amine factor was sought by examining the data for a dominant particle phase amine formation pathway, namely for signs of aqueous dissolution, acid-base reaction or oxidation (Ge et al., 2011). First, the Amine factor time series was examined relative to external measurements. Dissolution into water droplets was investigated by comparing the time series with periods of rain, fog, or high RH: no association could be identified as the Amine factor often appeared on clear days with lower RH. Reaction with acidic species was also considered through time series analysis of the extent of neutralization, a useful metric for determining periods of particle acidity. However, this metric cannot provide reliable information, as NO_3^- cannot be properly quantified prior to PMF analysis due to amine interferences. The temporality of the Amine factor was also investigated because the daytime maximum identified for a similar factor identified by Sun et al. suggested that photo-oxidation and condensation can also be a likely source (Sun et al., 2012). However, no consistent diurnal trend was noted. Docherty et al. reported similar difficulty in determining the origins of an amine related factor through time series analysis of results from a $PMF_{Org\ MS}$ analysis (Docherty et al., 2011).

Mass spectral comparison to laboratory generated amine MS provided better indication as to the chemical nature of the Amine factor. Among comparisons with mass spectra from suspected amine compounds reported in the NIST library, the Amine factor's profile was most similar to that of triethylamine (TEA: $C_6H_{15}N$, 101 g mol^{-1}), as demonstrated in Figure S 2.1 (r^2 = 0.23) (Stein, 2013). However, direct comparisons between AMS and NIST mass spectra are interpreted with caution, as they use different ionization techniques which can lead to mass spectral differences (Canagaratna et al., 2007a). Nonetheless, the amine spectra showed the same characteristic peaks (i.e., *m/zs* 56, 58, and 86).

Examination of AMS mass spectra of amines provided further perspective. Amines have been studied by AMS in chamber experiments to examine potential reaction pathways, for example oxidation, such as by nitrate radical (Silva et al., 2008; Malloy et al., 2009; Murphy et al., 2007), and reaction with acid gases such as HNO_3 (Silva et al., 2008; Murphy et al., 2007). These different mechanisms can actually lead to similar mass spectra (Malloy et al., 2009). The MS of the Amine factor in this study was determined to be very similar to that of TEAN reported by Murphy et al. (2007), resultant from reaction between TEA and HNO_3, with signal at *m/zs* 30, 46, 58, 86 and 100 (Murphy et al., 2007). One sign of reaction formation of amine salts from reaction with HNO_3, as reported by Malloy et al., is the presence of significant signal from NO^+ and NO_2^+ (at *m/z* 30 and 46) (Malloy et al., 2009). Examination of the MS from the Amine factor showed that signal was very high at *m/z* 30, and some signal was also present at *m/z* 46, although as mentioned previously, *m/z* 30 can also represent CH_4N^+, and CH_2O^+. There were no mass spectral signs to suggest an oxidation mechanism over salt formation. Ultimately, the factor was interpreted as being dominated by TEAN.

With this interpretation, an effective RIE for the factor was calculated. This was achieved by assuming a neutralized factor, and that TEAN was the only component. Though there did appear to be other contributions (e.g., SO_4^{2-}), these appeared very low. The nitrate fraction was calculated using the nitrate fragmentation pattern, with *m/z* 30 altered to reflect the isotopic ratio between *m/z* 30 and 46, obtained from calibration. The RIE of the amine fraction was determined by assuming factor neutrality, and that the remaining mass following subtraction of nitrate was triethylammonium. An RIE for the amine fraction of 6.0 was determined from this calculation, which fell within the range of RIEs previously measured for various amine salts. With the nitrate fraction taken into consideration, an effective RIE of 4.3 was established. This amine salt interpretation appeared to provide reasonable mass concentrations, as the calculated RIE resulted in spikes (<2hrs) reaching a magnitude of 4.8μg m^{-3}, while an RIE of 1.3 reflective of oxidized amines, resulted in concentrations exceeding 15μg m^{-3}. While the factor was assumed to be dominated by TEAN, its exact nature could not be validated; no amine fragmentation pattern proved an exact match, and external high time resolution collocated sub-micron PM mass measurements were not available to validate the RIE through PM mass comparison. In considering an acid-base chemistry, calculations by Murphy et al. have showed that the formation of aminium salts from the reaction of HNO_3 and TEA is only thermodynamically favorable in the presence of very low NH_3 (Murphy et al., 2007). These conditions may have been provided by plumes from a nearby source.

Four studies to date have identified an amine related factor through PMF of AMS mass spectra to the authors' knowledge (Aiken et al., 2009; Docherty et al., 2011; Hildebrandt et al., 2011; Sun et al., 2012). The analyses by Aiken et al., Docherty et al., and Hildebrandt et al. all extracted the amine factors from PMF of the organic MS, while Sun et al. extracted it from the full MS. Since the former three applied PMF to only the organic MS, significant mass that may have been associated with this factor (i.e., *m/z* 30) was potentially not captured. Furthermore, the latter study did not take into account the potential for a wide range of RIEs for the amine-related species, as highlighted by Silva et al. (2008), and discussed in this study. Regardless of the exact methodology, it can be seen that PMF can be effective in resolving atypical factors, such as amines.

3.1.2 Sulphate-OA factor

The time series and mass spectral profile of the Sulphate-OA factor are shown in Figures 4 and 5 respectively, and the chemical composition breakdown for this factor is shown in Figure 7. A mass spectral comparison between the Sulphate-OA factor and the published MS of atomized $(NH_4)_2SO_4$ (Hogrefe et al., 2004), shows that they exhibit the same major peaks at *m/z* 16, 17, 48, 64, 80, and 81, and compare well with an r^2 of 0.74. The Sulphate-OA factor on average contributed 1.81μg m^{-3}, or 25% to the sub-micron PM mass, and showed the highest mass concentrations towards the beginning of the campaign when air masses originated from the south. Overall, this factor showed a slight correlation with $PM_{2.5}$ mass concentration (r^2 = 0.21). A moderate correlation with SO_2 (r^2 = 0.31) implied that this factor was likely not only influenced by long range transport, but also by local sources. A more local influence was determined through examination of these temporal trends, which showed that several spikes in the Sulphate-OA factor coincided with large spikes (up to 58ppb) of SO_2. Local (within the metropolitan area) and local-to-regional (within ~ 100km) geographic origins for the Sulphate-OA factor were investigated by CPF. This highlighted a strong association with emissions from the southwest (Figure 8b), which was consistent with some local and local-to-regional coal fired power plants (Figure 1). Three large SO_4^{2-} spikes were observed on January 19th, 24th, and 27th: the first two were associated with the west-southwest, and the last with southeast, and all of which were likely associated with local coal-fired power plants. A smaller, yet still significant influence from the northeast was also observed, which may have been associated with emissions from coal plants located to the northeast. The aforementioned spikes were all associated with large excursions in SO_2 (24, 34, and 58ppb respectively), and each lasted about 2-6 hours. While the CPF on the whole demonstrated strong directionality to the southwest, this method cannot resolve how far away the responsible source(s) actually are located. Since southwesterly winds in Windsor are also consistent with typical synoptic flows for this region even in winter, and there are known large SO_2 emissions sources located further away in the Ohio River Valley, regional influences for the Sulphate-OA factor were also investigated using the PSCF (Figure 9a). The PSCF calculations for all factors were performed using data greater than the 50th percentile, but for the Sulphate-OA factor, the three spikes associated with more local emissions were removed. The PSCF highlighted high probability source regions around the Ohio River valley, an area known as a major SO_2 source due to the presence of many large coal fired power plants. A dominant regional influence was also demonstrated by a reasonably constant diurnal profile (Figure 11a). The geographic origins of the factor were also consistent with those of a Sulphate factor derived from a long-term receptor modeling study of Windsor (Jeong et al., 2011), and the nearby rural location of Harrow, Ontario (McGuire et al., 2011).

As the NH_4^+ and SO_4^{2-} contained within the Sulphate-OA factor likely formed an $(NH_4)_2SO_4$ salt, the extent of neutralization was calculated (Table 2). It was assumed that the only species capable of participating in the neutralization reaction, in this factor and in others, were NH_4^+, NO_3^-, SO_4^{2-}, and Cl^-. Aminium species were assumed to have been effectively separated into the Amine factor through PMF and thus it was assumed they did not contribute to the neutralization of other factors. The extent of neutralization ($Neut_{Ext}$), reported as the ratio of cations/anions in units of molar equivalents, was defined by:

$$Neut_{Ext} = \left(\frac{\frac{NH_4{}^+}{18}}{\frac{2SO_4{}^{2-}}{96} + \frac{NO_3{}^-}{62} + \frac{Chl}{35.5}} \right), \qquad (4)$$

where a neutral factor shows a $Neut_{Ext}$ of 1, and acidic factors show values less than 1.

The extent of neutralization of the Sulphate-OA factor was 0.99, indicating that the factor was reasonably neutral. It should be noted that a source of uncertainty in this value lies in the use of default RIE values for most species. Despite this potential uncertainty, the factor appeared neutral, similar to several other factors. Rotational analysis showed that the composition of this factor, and thus the degree of neutralization, did not change with FPeak rotations (Figure S-2.5). This suggested that regional rather than local sources of SO_4^{2-} had a greater influence on the chemical composition of this factor. While the Sulphate-OA factor appeared neutralized, simultaneous SO_2 and SO_4^{2-} spikes suggested contributions from more local, possibly primary SO_4^{2-} emissions sources, which may have been more acidic. As highlighted in Figure 10a, these SO_4^{2-} events, while high in mass, did not account for a significant fraction of the total sulphur due to the magnitude of the coincident SO_2 spikes (up to 65ppb, 1 min average). This could be attributed to the observed winter conditions that do not favor rapid oxidation of SO_2. Interestingly, a smaller SO_4^{2-} size distribution was observed during these spikes (from AMS p-ToF data), substantiating local SO_4^{2-} contributions. Figure 10b shows that SO_4^{2-} measured over the entire campaign showed an average modal size of 500nm (accumulation mode consistent with regional transport), while the size modes observed during the spikes were much smaller (150 – 250nm). These results indicate that proximate sources of SO_4^{2-} contributed to the total SO_4^{2-}, particularly during the largest SO_4^{2-} spikes.

Examination of the residuals from the six factor solution shows that some AMS signal cannot be accounted for during the Sulphate-OA factor/SO_4^{2-} spikes, indicating that another factor may be required to more fully explain the mass during these spikes. As a result, higher order solutions were investigated, and are reported in the supplementary material. Figure S-2.12 shows that at eight factors, the Sulphate-OA factor split into two factors: a Regional Sulphate factor that was characterized by synoptic-scale temporal rises, and a Local Sulphate factor that captured the SO_4^{2-} spikes. While the Local Sulphate factor appeared meaningful in that it captured residual SO_4^{2-}, the eight factor solution could not be justified for several reasons, which are further detailed in the supplement. First, while the Local Sulphate factor appeared acidic ($Neut_{Ext}$ = 0.25), consistent with more local origins, the Regional Sulphate factor in the eight factor solution now appeared over neutralized ($Neut_{Ext}$ = 1.27), relative to a reasonably unchanged, and neutral Nitrate-OA factor. Second, the OOA factor appeared split, resulting in an OA factor which did not show a strong enough resemblance to any known, ambient deconvolved OA. Finally, the correlation between the HOA factor MS from the eight factor solution and the reference HOA was worse than in lower order solutions. Mass spectral examination showed that more signal was apportioned to *m/z* 16 and 17 in higher order solutions; this effect was mainly attributed to solution uncertainty, as FPeak analysis of the six factor solution showed some variability in these fragments upon rotation. Although the Sulphate-OA factor from the six factor solution did not fully capture the variability and types of SO_4^{2-} observed, it appeared stable, with a low degree of rotational uncertainty (Figure S-2.5). It is possible that the Local Sulphate factor could be extracted more definitively if it were more prominent in the dataset. However, resolving acidic factors may not always be realistic, as data quality, receptor site complexity and atmospheric dynamics can all influence factor resolution. Nonetheless, resolving acidic factors could be useful from a parameterization perspective for resolving the effects of acidic aerosols on health, impacts on materials, or acidic seed particle chemistry, such as the competition between NH_3 and organic gas uptake to acidic SO_4^{2-} containing particles (Liggio et al., 2011; Liggio and Li, 2013).

The organic fraction of the Sulphate-OA factor was extracted for comparison with the organic fraction of other factors, as well as published organic factor MS (Figure 6). Uncertainty in the organic fraction was assessed through rotational analysis, and was found to be low suggesting that these organics were reasonably rotationally fixed. The organic composition amongst factors extracted using the $PMF_{Full\ MS}$ analysis was assessed against that from other studies. Only one of the past three similar studies, that of Sun et al., (2012), was sufficiently similar for comparison; Chang et al., involved Arctic aerosol, and the analysis by Crippa et al., only involved the organics and SO_4^{2-}. The Sulphate-OA factor contained 21% organics by mass, accounting for 16% of the total measured organics; interestingly this value was the same as that produced in the analysis by Sun et al., (2012). Although both of these studies were conducted in highly urban environments, such an agreement is interesting, considering that different organic factors were found. Compared to other factors from this study with significant organic content (i.e., > 15% by mass), the Sulphate-OA factor organics were most similar to typical OOA mass spectra, and were the most highly oxidized according to the associated F44 and O/C ratio. The F44 metric (fractional contribution of *m/z* 44 within the organic MS) has been used in $PMF_{Org\ MS}$ studies to assess the degree of oxygenation of OOA factors, as it primarily represents CO_2^+, the most prevalent oxygenated fragment within the organic MS. An empirical relation between F44 and the atomic oxygen to carbon ratio (O/C) within a PMF OOA factor has been developed based on a collection of laboratory and field study data (based on $PMF_{Org\ MS}$ analyses) (Aiken et al., 2008), and has been used to estimate the O/C ratio for similar factors in other studies, including previous PMF studies of combined organic and inorganic mass spectra (Chang et al., 2011;Sun et al., 2012;Crippa et al., 2013b). An F44 of 0.15 (estimated O/C = 0.65) was calculated for this factor, the highest value from this study and consistent with the average values obtained for OOA for two-component OA datasets (i.e. HOA and OOA) across the Northern Hemisphere (F44 = 0.14 ± 0.04, O/C = 0.62 ± 0.15, mean ±1σ) (Ng et al., 2010).

Many previous AMS PMF studies have shown that a high degree of correlation exists between SO_4^{2-} and OOA (Lanz et al., 2008; Ulbrich et al., 2009; Slowik et al., 2010; Richard et al., 2011). However, this analysis has been useful for sub-apportionment of the oxygenated organic fraction of OA to different factors, as the Sulphate-OA factor was found to contain a notable fraction (31%) of the total OOA (defined here as the proportion of *m/z* 44 signal apportioned to this factor, excluding the Amine factor), and in this case, the most oxidized fraction of the OOA. The higher degree of oxygenation exhibited by this factor is consistent with its regional origins from the south, and a longer atmospheric lifetime. Although the mixing state of particles associated with this factor cannot be positively deduced from these data, two extremes exist. Either this factor mainly represents externally mixed OOA and

$(NH_4)_2SO_4$ particles that exhibit similar temporality due to regional transport, or it represents internally mixed $(NH_4)_2SO_4$ particles coated by lower volatility SOA during regional transit.

In summary, the Sulphate-OA factor was neutralized and associated with the most highly oxygenated organics. Cross-apportionment of the most oxygenated organics measured during this campaign further reinforced this factor's aged, regional nature. While the Sulphate-OA factor appears to be dominated by regional transport of neutralized ammonium sulphate, minor contributions from more local, primary SO_4^{2-} sources were present as well.

3.1.3 Nitrate-OA factor

The Nitrate-OA factor time series and mass spectrum are shown in Figures 4 and 5 respectively, and its contribution to total mass is shown in Figure 7. Of all the factors, it contributed most to the sub-micron PM mass, with an average mass concentration of 3.19µg m^{-3} (45%). Significant accumulation was observed towards the end of the campaign, when a severe nitrate episode occurred, and this factor's mass alone exceeded 20µg m^{-3}.

Deconvolution of the Nitrate-OA factor into its component species (Table 2) shows that it was mostly composed of NH_4^+ and NO_3^- (78% by mass). However, other species such as organics and SO_4^{2-} also comprise a significant mass fraction (16% and 6% respectively). As with the Sulphate-OA factor, the Nitrate-OA factor demonstrated identical organic composition to the NO_3-OA factor found in the study by Sun et al., (2012). That both of these largely inorganic factors were highly similar to another study conducted in New York City is a possible indication of consistent internal and/or external mixing between these combined inorganic and organic species in these types of inorganic factors. The dominance of ammonium nitrate in this factor's mass spectrum was confirmed by a high correlation with published NH_4NO_3 standard spectra (r^2 = 0.96) with peaks at *m/z* 17, 18, 30, and 46 (Hogrefe et al., 2004). Comparison with NH_4NO_3 calibration mass spectra showed that it also compared well, although the factor's *m/z* 30 to 46 ratio was 19% higher than the calibration mass spectrum, which was likely due to the presence of organics. The Nitrate-OA factor contained 20% of the total measured organics during the campaign, or 31% of the oxidized organics (as defined by the fraction of *m/z* 44 apportioned to this factor). The nitrate-bound organics displayed the second highest F44 (0.12) of all the factors from the $PMF_{Full\ MS}$ analysis. The F44 of 0.12 corresponded with an estimated O/C = 0.54, which when compared to OA components from $PMF_{Org\ MS}$ studies, falls between typical values for OOAI and OOAII indicating moderately oxidized organics (Ng et al., 2010). Several previous $PMF_{Org\ MS}$ studies have found an association between NO_3^- and OOAII, suggestive of temperature dependent volatility (Lanz et al., 2007; Ulbrich et al., 2009). The diurnal trend for the Nitrate-OA factor partly suggests semi-volatile behavior, due to a slight inverse relationship with temperature (Figures 11b and e), however slightly higher nighttime values may also be associated with decreased mixing. As a stronger inverse relationship was noted for the OOA factor than Nitrate-OA, it was likely that the Nitrate-OA factor was likely more regionally influenced. This was reinforced by an *m/z* 44 to 43 ratio of 1.5, which was lower than that for the Sulphate-OA factor, yet still higher than that expected for OOAII. The extent of neutralization shows that the ratio of cations to anions was near unity (1.04), suggestive of a reasonably neutral factor. FPeak rotational analysis demonstrates that the Nitrate-OA factor appears rotationally fixed (Figure S-2.5).

Sources of NH_4NO_3 precursor gases (i.e., NH_3 and NO_x) in the Windsor region are abundant: constant vehicle traffic, in large part from the nearby border crossing, provides a constant supply of NO_x (38.0 ± 35.0 ppb), as well as minor contributions of NH_3 (Li et al., 2006; Godri et al., 2009). While the Windsor/Detroit area may not comprise as significant a source region for NH_3 as rural agricultural areas, many point industrial (e.g., wastewater reclamation plant) and diffuse (e.g., traffic, population) sources do emit large quantities of NH_3. According to Environment Canada's NAPS monitoring network, NH_3 levels are lowest in wintertime in Windsor, yet are still detectable: using the multi-year average NH_3 wintertime concentration measured by ion chromatography, the average wintertime NH_3 concentration in downtown Windsor between 2004 and 2007 was 0.5 ± 0.6 ppb, which exceeds the 0.1 ppb detection limit for this analytical method. Figure 11b presents the diurnal trend for the Nitrate-OA factor. Noted along with a slight diurnal profile that was likely influenced by both temperature (Figure 11b), as well as reduced mixing overnight and into the early morning, were two small peaks consistent with morning and afternoon rush-hour traffic, at 09:00 and 17:00. These peaks were likely due to NH_4NO_3 formation from traffic emissions. A more general traffic contribution to the Nitrate-OA factor was observed by moderate and slight correlations with black carbon (BC) (r^2 = 0.31), and NO (r^2 = 0.17) respectively, both traffic tracers.

The geographic origins of the Nitrate-OA factor were explored. The CPF, presented in Figure 8c, did not reveal any significant directionality; this indicated that this factor was not significantly influenced by any local point sources, but did not discount potential contributions from local diffuse sources, such as traffic. The regional nature of the factor was explored through the PSCF (Figure 9b), which highlighted areas of high source probability to the south and southwest. In comparison with the PSCF from the Sulphate-OA factor, the Nitrate-OA factor also appeared more regionally influenced than the Sulphate-OA factor, yet from less specific source regions. Regional influences are more likely in winter compared to summer in this location, as nitrate can persist and be transported greater distances provided cold enough temperatures. In summary, the Nitrate-OA factor contributed most to sub-micron PM mass, was associated with moderately oxidized organics, and was likely attributed to both local and regional sources, with regional contributions likely dominating.

3.1.4 Chloride factor

Presented in Figures 4 and 5 respectively are the time series and mass spectral profile of the Chloride factor. The chemical composition breakdown for this factor is shown in Figure 7. Strong peaks observed at *m/zs* 16 and 17 indicate significant NH_4^+ content, while peaks at *m/zs* 35, 36, 37 and 38 indicate chloride. The factor appeared to be dominated by NH_4Cl, as it compared well with the NIST mass spectrum for this species ($r^2 = 0.71$). The isotopic ratio of *m/z* 35 to 37 matched that from the AMS chloride fragmentation pattern (3.09). Application of the AMS fragmentation table to the MS demonstrates that NH_4^+ and Cl^- contributed 28% and 27% respectively to the mass of this factor, however, other species were also evident, namely NO_3^- (13%), organics (13%) and SO_4^{2-} (18%). This study represents the first PMF analysis of AMS mass spectral data to apportion NH_4^+ and Cl^- to a unique factor suggestive of mostly ammonium chloride. The extent of neutralization (1.09) shows that this factor was fairly close to neutral, taking into account all identifiable ions (i.e., NH_4^+, Cl^-, NO_3^-, and SO_4^{2-}), and considering potential PMF error and uncertainty in RIEs.

Interestingly, the factor was composed 13% by mass of organics (Figure 6). The most significant organic peaks were *m/z* 29, 41, and 55, and mass spectral delta pattern, with a $\Delta = 0$ (i.e., *m/z* 27, 41, 55, 69, etc.) was noted (McLafferty and Tureček, 1993). However, despite a distinct delta pattern, the factor showed rotational uncertainty that precluded over-interpretation of the factor's organics. With negative rotations, the Cl^- and NH_4^+ content varied only slightly. However, rotation in both the positive and negative direction caused significant changes to the organic fraction delta pattern: negative rotations caused the $\Delta = 0$ pattern to decrease and the $\Delta = 2$ (*m/z* 29, 43, 57, 71, etc.) to increase, while there was insignificant change in the organic mass spectral profile with positive rotations. As the organic profile and content varied most significantly among all of the Chloride factor components (from 18% to 40% by mass), the delta pattern could not be used with confidence for factor identification. It should be noted that little uncertainty was observed for the SO_4^{2-} mass fraction of the Chloride factor, indicating that the SO_4^{2-} cross-apportionment was relatively robust. Although the Chloride factor showed the most uncertainty among all PMF factors (Figure S-2.5), its appearance from five to eight factors suggested it was robust.

The presence of NH_4Cl aerosol in the atmosphere has previously been noted. Pio et al. performed early experiments to assess thermodynamic behavior of NH_4Cl under tropospheric conditions and found that like NH_4NO_3, NH_4Cl formation is favored by lower temperatures and higher RH (Pio and Harrison, 1987a, b). The conditions associated with the Chloride factor were examined (i.e., temperature, RH, cloudiness, fog, rain), to determine if rapid meteorological changes triggered gas to particle transition. No association could be discerned. However, it should be noted that from January 14th onward, on the whole, the conditions for NH_4Cl were favorable with a mean temperature of -8 ± 5ºC, and RH of 73 ± 13%.

Although not directly measured, particulate NH_4Cl has been speculated to be present in several settings due to high correlation between its component species. Perron et al. have reported NH_4Cl-containing particles in a Swiss alpine valley setting due to significant correlation in NH_4^+ and Cl^- spikes, with Cl^- likely emitted as KCl during biomass combustion (Perron et al., 2010). In a study in Mexico City, Salcedo et al., reported large, yet short-lived plumes of chloride, which were coincident with spikes in both NH_4^+ and organics; the simultaneous appearance of both NH_4^+ and Cl^- indicated NH_4Cl formation (Salcedo et al., 2006). Precursor gases (e.g., NH_3, HCl, and HNO_3) and their sources are plentiful in this region. Although NH_3 is typically the limiting agent in these reactions, in this region, point industrial (e.g., wastewater reclamation plant), and diffuse sources (e.g., traffic, population) of NH_3 are numerous. There are thus two plausible mechanisms for NH_4Cl formation in the Windsor/Detroit region. In the first case, NH_3 could react with primary HCl which has been emitted directly by anthropogenic sources. According to TRI and NPRI emissions inventories, the largest primary emitter of HCl in Windsor/Detroit in 2005 was the River Rouge Power Plant, located 3km southwest of the receptor site (US EPA, 2013). However, secondary reactions may lead to HCl production, and eventually NH_4Cl formation as well. It is possible that acidic, ammonia poor, industrial plumes with sufficient HNO_3 content may liberate HCl from certain sources, which then subsequently repartitions as NH_4Cl to the particle phase under NH_3 rich conditions. Some of these sources include NaCl particles from road salt and KCl from biomass burning emissions (including coal combustion and domestic wood burning). Waste incineration has also been identified as a potential source of short duration, strong chloride events; Moffet et al. reported Cl^- spikes alongside with spikes in Zn and Pb-containing particles measured by ATOFMS in Mexico City (Moffet et al., 2008a;Moffet et al., 2008b). These events were attributed to rapid secondary HCl formation from the reaction of HNO_3 with PbCl and ZnCl in a waste incineration plume. All of these sources were likely in this study: as mentioned previously, there are several coal plants near the site, and a waste incinerator is located to the northwest. Furthermore, given the winter-time conditions, domestic wood burning was prevalent in the region.

Examination of the CPF (Figure 8d) and PSCF (not shown) did not provide any additional information with respect to local or regional source origins. However, concurrent appearance of sharp spikes in Cl^- and SO_4^{2-} (Figure 3), and moreover the apportionment of significant SO_4^{2-} to this factor suggested an association with industrial emissions. Both of these spikes corresponded with a 230-250º wind direction, consistent with coal plants to the west-southwest. Despite these spikes having been partially captured by their respective, reasonably neutralized PMF factors, the Cl^- and SO_4^{2-} observed in these spikes was likely not well neutralized, as concurrent spikes in NH_4^+ at these times were not as strong as those observed for its counter ions. Any available NH_3 at this time was likely partitioned as $(NH_4)_2SO_4$ first, because $(NH_4)_2SO_4$ formation should be thermodynamically more favorable than NH_4Cl formation under the given meteorological conditions. As such, while the Chloride factor appeared reasonably close to neutral on the whole, there was likely some variation in acidity that was not captured by this factor, as more acidic particles appeared to be present during the spikes. Furthermore, the rotational uncertainty determined through FPeak analysis may have been an indication of the more dynamic nature of this factor's components. In summary, the Chloride factor was most likely associated with local atmospheric processing, whereby ammonium chloride secondary aerosol formed rapidly in-plume from the reaction of NH_3 and HCl emissions. The source for HCl emissions may have been primary emissions from an industrial facility, and/or it may have formed from secondary reactions.

3.1.5 HOA factor

A hydrocarbon-like organic factor (HOA) was extracted by PMF and its time series and mass spectral profile are presented in Figures 4 and 5 respectively. The factor's chemical composition is shown in Figure 7. Accounting for 0.94 µg m^{-3} or 13% of the sub-micron PM mass during the campaign, the HOA factor represented the third largest contributor to sub-micron PM mass. Delta patterns of Δ=0 and Δ=2 were observed in the mass spectral profile, most likely corresponding to alkanes and H_2-neutral losses from alkyl fragments and/or alkenes, respectively (McLafferty and Tureček, 1993;Zhang et al., 2005). The extracted HOA factor was similar to those from the Pittsburgh fall 2002 (Ulbrich et al., 2009), and the Zurich winter 2006 (Lanz et al., 2008) studies, with r^2 values of 0.56 and 0.66 respectively.

Deconvolution of the HOA MS into organic and inorganic species was performed using the AMS fragmentation table. Contributions from NH_4^+ (5%) and NO_3^- (9%) were noted, indicating that this factor was likely mixed with NH_4NO_3. FPeak rotational analysis shows that although contributions of these species were moderate, their variation with rotation precluded their over-interpretation (Figure S-2.5). A less than plausible extent of neutralization of 1.62 also served to highlight the rotational ambiguity associated with the inorganics, although this uncertainty could be a result of low overall inorganic contributions. With an organic composition of 85%, it was not as similar to the HOA factor found in Sun et al. (97%), as it was for other factors.

HOA is often referred to as a surrogate for fossil fuel combustion emissions, with traffic cited as the most significant source contributor (Aiken et al., 2008). The same can be said for this study; moderate r values of 0.48, and 0.64 were found between the HOA factor with BC and NO respectively, pollutants which are typically associated with relatively fresh traffic emissions. The HOA factor also displayed moderate and slight correlations with CO (r^2 = 0.41), particle number concentration (r^2 = 0.21), and aromatic hydrocarbons measured by PTR-MS, such as benzene (*m/z* 79, r^2 = 0.43), toluene (m/z 93, r^2 = 0.32), C_2 - benzene (*m/z* 107, r^2 = 0.58), and C_3 - benzene (*m/z* 121, r^2 = 0.54), which are also typically associated with primary anthropogenic emissions, such as traffic (Vlasenko et al., 2009). Distinct rush hour peaks in the morning (05:00 – 09:00) and evening (18:00 – 22:00) further supported source attribution to traffic emissions (Figure 11c). The CPF for the HOA factor provides modest support for a traffic source, as excursions in this factor were moderately associated with the north-east wind sector (0 - 90º), consistent with higher traffic density from the international border crossing (Figure 8e). While general circulation traffic is also likely to be a significant contributor to the HOA factor, many industrial operations in the region combust fossil fuels in their processes, for instance heavy machinery used for onsite material transport. As such, other sources may also contribute to this factor. Thus, the HOA factor represented primary organic aerosol emissions, with its most significant contributions likely emitted from traffic.

3.1.6 OOA factor

A factor consistent with oxygenated organic aerosol (OOA) was extracted using $PMF_{Full\ MS}$, and its time series and MS are presented in Figures 4 and 5 respectively. On average, the OOA factor comprised 0.76μg m^{-3} or 11% of the sub-micron PM mass. The fragmentation table was applied to this factor to decouple the inorganic and organic species for species-based mass spectral and temporal examination. The only other species associated with this factor was NO_3^- (7% by mass). While the OOA factor represented the lowest F44 compared to Sulphate-OA and Nitrate-OA (F44 = 0.09), it contained the highest fraction of oxygenated organic aerosol, as 35% of *m/z* 44 was apportioned to this factor. The robustness of the factor mass spectrum was examined using FPeak analysis. It was found that rotations caused the minor NO_3^- concentration to vary (Figure S-2.5). With a lack of neutralizing species (i.e., NH_4^+) present, the nitrate contribution may have been attributed to model error. In examining the robustness of the F44 content through FPeak analysis (Table S2.1), it varied only slightly, suggesting minor rotational ambiguity with respect to the oxygenated organic fragments. In terms of organic composition, this factor's organic composition (93%) was most comparable to the LV-OOA factor from Sun et al., (2012), which comprised 94% organics.

Comparing this F44 value with previous studies, it is apparent that the F44 observed in the OOA factor in this study is lower than others from two component organic results (Ng et al., 2010). This observation highlights a distinct difference in $PMF_{Org\ MS}$ vs. $PMF_{Full\ MS}$. Typically, the contribution of *m/z* 44 to the total organic spectrum is highest in the OOA factor when PMF is applied to only the organic MS. However, in this study it represents the third most oxygenated organic component among the PMF factors, yet the highest contributor to oxygenated organic aerosol. Comparing with mass spectral profiles from other studies, this OOA factor more closely resembled semi-volatile OOAII factors, instead of highly oxygenated OOAI factors, given the comparatively low *m/z* 44/43 ratio. The diurnal trend provided further insight into the nature of the OOA factor (Figure 11d). It can be seen that this factor was significantly higher overnight than during daylight hours, suggesting either buildup in concentration in the nighttime boundary layer, or semi-volatile nighttime gas to particle partitioning. The latter was suspected, as lower concentrations were observed on warmer nights, suggestive of a temperature/volatility concentration dependence. In addition, the OOA factor exhibited a stronger anti-correlation with temperature than the Nitrate-OA factor (r = -0.26), suggesting that temperature played a greater role in explaining the variability in the OOA factor than in the Nitrate-OA factor. This was evident in increased contributions in the OOA factor mid-way through to the end of the campaign, when the air was colder. These results show that less oxygenated, and thus likely more local and semi-volatile OOA, appeared to be a significant fraction of the total oxygenated organic aerosol.

The moderately oxidized and semi-volatile behavior of the OOA factor was further demonstrated through the highest correlation amongst all factors with acetaldehyde (r^2 = 0.31), a VOC with an atmospheric lifetime of less than a day. Slowik et al., also report observing high correlations between a semi-volatile, OOAII factor and acetaldehyde in Toronto, ON (Slowik et al., 2009), and a similar conclusion can be drawn here that this factor's variability is influenced by both oxidation timescale as well as gas-particle partitioning. Ultimately, this factor more closely resembles OOAII rather than OOAI.

The geographic origins of the OOA factor were investigated by both CPF and PSCF. The CPF, shown in Figure 8f, shows a similar result as was found for the HOA factor, with a moderate association with emissions to the north-east, suggestive of contributions from traffic. However, on the whole, no strong directionality was observed, supporting local oxidation of organic aerosol. The PSCF for this factor was also generated (not shown), although no distinct source regions could be identified, reinforcing the notion that transport was not responsible for the temporal behavior of OOA in Windsor's winter-time air. Hence, the OOA factor mainly represented local atmospheric processing, and appeared to be characterized by less oxygenated, semi-volatile organic aerosol.

3.2 PMF$_{\text{Full MS}}$ vs. PMF$_{\text{Org MS}}$

As only two other studies to date have performed PMF on the complete or near complete MS, the following section investigates the effect of including both inorganics and organics in the analysis. The two to six factor solutions from PMF$_{\text{Org MS}}$ were examined and compared to the six factor PMF$_{\text{Full MS}}$ solution. Based on the mass spectral profiles and PMF diagnostics, the three factor solution provided the most physically meaningful results. A two factor solution generated Amine and OOA factors, and moving to a three factor solution produced Amine, OOA and HOA factors similar in profile to those from the PMF$_{\text{Full MS}}$ analysis. Adding a fourth factor caused the OOA factor to split, leading to another with an MS which did not sufficiently resemble any known factors (nor any of the organic fractions contained within the factors from the $PMF_{Full\ MS}$ solution). The same applied to the five and six factor solutions. A comparison between higher order solutions from the $PMF_{Org\ MS}$ analysis and the organic fraction of the $PMF_{Full\ MS}$ six factor solution showed that they did not contain the same information, indicating that organics were resolved differently between the analyses. As the three factor solution led to the most physically meaningful results, it was compared with the six factor $PMF_{Full\ MS}$ solution, and is discussed below. The three factor solution justification, along with descriptions of the four to six factor solutions are presented in the supplement.

Overall, the organic fraction was mainly split into the HOA and OOA factors, whereby these factors each contributed 53 and 47% relatively to the total OA as assessed by the $PMF_{Org\ MS}$ analysis. This nearly 50:50 division between these two organic components was somewhat different than that found in other two component studies in urban areas, with HOA making a greater contribution (Zhang et al., 2007). Such a difference could possibly be attributed to the significant industrial activity and traffic contributions from the international border crossing.

3.2.1 Amine factor comparison

The mass spectra of the Amine factors extracted from the two PMF analyses are compared in Figure 12a. The most notable difference between the two profiles was the presence of a significant contribution from *m/z* 30 in $PMF_{Full\ MS}$ analysis. The majority of this signal was removed during extraction of the organic MS as it is mostly attributed to NO^+ in the fragmentation table. Excellent agreement was found between the factor time series (r^2 = 0.99), indicating that this factor was similarly extracted in the two analyses (Figure 13a).

The extraction of the Amine factor in this study highlights advantages of applying PMF to the full AMS mass spectrum for unit mass resolution data. Firstly, it can be seen that PMF can provide better resolution of AMS species (i.e., SO_4^{2-}, NO_3^-, NH_4^+, Cl^-, organics) than using the traditional AMS fragmentation scheme, as this method does not pre-assume the nature of chemical species. In this study, the presence of the Amine factor had consequences for the estimation of organics mass concentrations, and ultimately sub-micron PM mass. A comparison between the AMS resolved species calculated pre-PMF with those calculated from the factors post-$PMF_{Full\ MS}$ analysis (excluding any mass associated with the Amine factor) is presented in Table 1. It can be seen that organics may have been overestimated by up 11%. Although the $PMF_{Org\ MS}$ analysis could be improved by stoichiometrically fixing the contribution of the subtracted inorganic component of *m/z* 30 (NO^+) to *m/z* 46 to include amine ions in the analysis, this was not performed for this analysis in order to highlight the potential benefits of using the $PMF_{Full\ MS}$ method (namely that no a priori assumptions are required regarding the chemical nature of the aerosol). Ultimately, when comparing the pre-PMF sub-micron PM mass to the post-PMF reconstructed mass, it can be seen that the mass may have been overestimated by up to 5% using the traditional fragmentation scheme.

Second, PMF of the full MS also provided better factor resolution and mass estimates than PMF of the organic MS; with $PMF_{Org\ MS}$, the organic MS was extracted through application of the organic fragmentation pattern, while in the $PMF_{Full\ MS}$ analysis, the full MS remained as measured, except for subtraction of air and water. Comparison between the $PMF_{Full\ MS}$ and $PMF_{Org\ MS}$ Amine factor time series showed that the mass of the Amine factor from the $PMF_{Org\ MS}$ was 2.6 times greater than that from the $PMF_{Full\ MS}$ analysis. This difference accounted for both the differences in RIE (an effective RIE of 4.3 was assumed in the $PMF_{Full\ MS}$ analysis), as well as mass contributions from other fragments (namely *m/z* 30, which is typically associated with nitrate but may also represent amines). A more direct comparison between the Amine factors resolved in the $PMF_{Full\ MS}$ and $PMF_{Org\ MS}$ analyses using $NO_3^-{}_{eq}$ mass showed that the factor resolved in the $PMF_{Full\ MS}$ analysis contained 25% more mass, given inorganic contributions. This suggests that some factors may not be fully resolved using the $PMF_{Org\ MS}$ method. As amine species were assigned as organics in the $PMF_{Org\ MS}$ analysis (with an RIE of 1.4 as opposed to 4.3), it can be seen that errors of up to two and a half times the mass may arise from not considering alternate possibilities for the chemical nature of certain species, which may become clearer through the extraction of the factor's full MS. It is possible that in some cases (e.g., amine rich areas with amines of higher RIE), this type of error could outweigh other AMS errors such as collection efficiency.

3.2.2 HOA factor comparison

Figure 12b presents the mass spectral comparison between the HOA factors resolved from PMF analysis of the full MS vs. the organic MS. The HOA factor mass spectra from the two PMF analyses compared very well (r^2 = 0.98), and good agreement was also found between their time series (r^2 of 0.98); a slope of 0.91 for the time series comparison indicated that a portion of this factor had been cross-apportioned to other factors in the full MS analysis (Figure 13b). Due to minimal differences between MS, it was difficult to distinguish across which factors this HOA was further distributed in the $PMF_{Full\ MS}$ analysis.

3.2.3 OOA factor comparison

Figure 12c provides a comparison between the OOA factor profiles extracted in the $PMF_{Full\ MS}$ and $PMF_{Org\ MS}$ analyses. Enhanced cross-apportionment of *m/z* 44 to other factors in the $PMF_{Full\ MS}$ analysis is evident due to the significant difference in the relative contributions of F44 in the OOA factors (i.e., $PMF_{Full\ MS}$ F44 = 0.09, $PMF_{Org\ MS}$ F44 = 0.15). An F44 = 0.15 found in the $PMF_{Org\ MS}$ in this factor is comparable to that found in other studies, also indicative that this factor included the highly oxidized organics that were separated into the Sulphate-OA factor in $PMF_{Full\ MS}$. Comparing the time-series of the OOA factors between the $PMF_{Full\ MS}$ and $PMF_{Org\ MS}$ analyses, a comparatively low r^2 = 0.72 highlighted that some OOA signal was cross-apportioned to inorganic factors in the $PMF_{Full\ MS}$ analysis (Figure 13c). A mass difference was also observed between the factors, with the $PMF_{Full\ MS}$ weighing on average 0.76μgm^{-3}, and the $PMF_{Org\ MS}$ measuring on average 1.01μgm^{-3}. A higher mass attributed to the $PMF_{Org\ MS}$ OOA factor is likely linked with the higher contribution from *m/z* 44. A comparison of just the organic contributions from the factors containing oxidized organic aerosol (Nitrate-OA, Sulphate-OA and OOA) with the OOA factor from the $PMF_{Org\ MS}$ three factor solution showed that the r^2 was much improved from 0.72 to 0.94 with the additional variability from the organic component of these factors (Figure 13d). A slope slightly higher than unity suggested that the organic aerosol extracted from these three factors was likely not entirely oxidized organic aerosol as defined from the OOA factor from the $PMF_{Org\ MS}$ analysis, and may have contained some less oxidized aerosol as well. This was corroborated by a slope of slightly less than unity for the HOA factor comparison.

Interestingly, the OOA factor could not be split into more OOA factors (i.e., OOAI and OOAII) using PMF analysis of the organics alone. Moving to a four factor solution resulted in an OOA factor, and an Other OA factor, which could not be fully justified, as its mass spectrum did not sufficiently resemble any known mass spectra to accept the solution (see supplement for further details). It is likely that the inorganics in the $PMF_{Full\ MS}$ analysis are providing additional correlational structure to more effectively apportion organics. If moderately oxygenated organics are calculated as those apportioned to the OOA and Nitrate-OA factors, and highly oxygenated organics are those apportioned to the Sulphate-OA factor, it can be seen that highly oxygenated organics comprise only about a quarter of the total oxygenated organics. With the low prevalence of highly oxygenated organics observed in this campaign, these species may not have carried sufficient weight in the model to result in the splitting of the OOA factor in the $PMF_{Org\ MS}$ analysis into OOAI and OOAII types. With the OOA dominated by moderately oxidized organics, the addition of the inorganics introduced correlational structure for these more minor, more oxidized OAA types could be isolated.

The effect of having performed PMF on the full MS is evident when comparing the time series between SO_4^{2-} and the $PMF_{Full\ MS}$ and $PMF_{Org\ MS}$ OOA factors. In many previous studies, particularly in urban locations, the OOA factor from PMF of the organic MS has been highly correlated with SO_4^{2-}. Here an r^2 of 0.38 was found between SO_4^{2-} and OOA from PMF of the organic fraction. However, following PMF of the full MS, the correlation between the $PMF_{Full\ MS}$ OOA factor and SO_4^{2-} was markedly lower (r^2 = 0.08). Thus, the $PMF_{Full\ MS}$ OOA factor shows a different temporal character, due to removal of the highly oxidized contribution. The remaining OOA that characterizes this factor thus more resembles the OOAII typically found when two OOA factors are extracted during $PMF_{Org\ MS}$. Thus, apportionment of organics of varying degrees of oxidation was more effectively accomplished through the $PMF_{Full\ MS}$ over the $PMF_{Org\ MS}$ method, most likely due to correlations with inorganic species of differing atmospheric behavior (e.g., volatility), and origins.

4 Conclusions

Six factors were identified through PMF analysis of the full AMS mass spectrum: an Amine factor suspected to be triethylamine nitrate; a Sulphate-OA factor composed of mostly $(NH_4)_2SO_4$ and highly oxidized organics; a Nitrate-OA factor consisting of mostly NH_4NO_3 along with moderately oxidized organics; a Chloride factor hypothesized to be mostly NH_4Cl along with organics and sulphate; an HOA factor classified as mostly primary organics from fossil fuel combustion; and an OOA factor, consisting of moderately oxidized organics.

Factor variability was governed by chemical processing, primary source emissions, and transport. The OOA factor appeared to be mostly influenced by local processing as it exhibited a strong nighttime diurnal trend consistent with gas to particle partitioning. While both the Amine and Chloride factors showed temporal trends with brief excursions suggestive of primary source emissions, rapid secondary aerosol formation could not be ruled out in either case. Rapid in-plume secondary formation of the Chloride factor was supported by its sporadic appearance, and concurrent appearance with short-lived spikes in SO_4^{2-}, consistent with industrial emissions plumes. While the precise mechanism of formation for the Amine factor could not be validated, it was hypothesized to be a result of acid-base reaction of primary triethylamine gaseous emissions with HNO_3. Two significant industrial sources of amines located to the southwest of the measurement site were likely the main contributing sources. By contrast, the main determinant for the HOA factor was primary source emissions, given its strong daytime diurnal trend, and high correlations with short-lived traffic related gases, such as NO. Regional transport was most likely the dominant determinant for variability for the Sulphate-OA and Nitrate-OA factors, although local gas to particle partitioning also appeared to contribute to the Nitrate-OA factor.

Allowing for PMF to cross-apportion inorganic and organic species between factors led to richer conclusions regarding the potential sources, chemical nature, and behavior of certain factors than would otherwise have been obtained through application of PMF of organics only. First, cross-apportionment of inorganic species between factors led to some enhanced aerosol chemistry conclusions, such as the relative degree of neutralization of co-varying inorganic species. It was found that NH_4^+ was cross-apportioned to the Sulphate-OA, Nitrate-OA and Chloride factors, and on the whole, each of these factors appeared reasonably neutral, at least relative to one another. In an eight factor solution, a more acidic Local Sulphate factor appeared. While this solution on the whole could not be justified, it suggests that acidic factors could be extracted in other studies. Second, inclusion of inorganics led to enhanced apportionment of organic aerosol, which in turn led to a better understanding of each factor's degree of oxygenation and chemical nature. For instance, less oxygenated organics were associated with the Chloride and HOA factors, which supported local, primary emissions sources. Inclusion of the inorganics also provided additional correlational structure to apportion the oxygenated organic fraction, with the most highly oxygenated OA apportioned to the regional Sulphate-OA factor, and the moderately oxygenated OA apportioned to the Nitrate-OA and OOA factors. Using this technique, the resulting OOA factor displayed behavior typical of temperature-dependent gas to particle partitioning, while the more oxidized organics contained in the Nitrate-OA and Sulphate-OA factors appeared longer lived, and more associated with regional transport. Without the inclusion of inorganics, the highly oxygenated and moderately oxygenated organics could not be effectively separated.

The methodology used in this study also proved advantageous for extracting atypical factors, and for obtaining more accurate mass quantification for data obtained from a unit mass resolution AMS. In this study, PMF of the full MS resulted in the extraction of the Amine factor, which was only partially extracted using PMF of only the organic MS. A more complete mass spectral profile including inorganic fragments (e.g., *m/z* 30) was extracted, which permitted further exploration into the factor's chemical nature. Although its formation mechanism could not be positively validated, the Amine factor was ascertained to have resulted from an acid-base neutralization reaction, and a factor specific relative ionization efficiency was calculated to provide improved mass estimates. This method was useful for preventing overestimation of certain species, such as nitrate, when the aerosol is influenced by species unaccounted for by the typical AMS analysis scheme. It is likely that this method would be even more useful for HR-ToF-AMS data, due to the ability to better understand the chemical nature of atypical factors from high resolution mass spectra. In summary, PMF of the full AMS unit mass resolution MS has been shown to be a useful method to obtain additional insights into the sources and processes governing fluctuations in non-refractory sub-micron PM chemical composition, in comparison to PMF of the organics alone.

Acknowledgements

These measurements were supported by Environment Canada. Funding for SOCAAR was provided by the Canadian Foundation for Innovation, the Ontario Innovation Trust, and the Ontario Research Fund. MLM is grateful to Environment Canada for funding this analysis through the Research Affiliate Program (RAP). The authors gratefully acknowledge the NOAA Air Resources Laboratory (ARL) for the provision of the HYSPLIT transport and dispersion model and/or READY website (http://www.arl.noaa.gov/ready.php) (Draxler and Rolph, 2010; Rolph, 2010) used in this publication. The authors also thank anonymous referees for helpful comments.

References

Aiken, A. C., Decarlo, P. F., Kroll, J. H., Worsnop, D. R., Huffman, J. A., Docherty, K. S., Ulbrich, I. M., Mohr, C., Kimmel, J. R., Sueper, D., Sun, Y., Zhang, Q., Trimborn, A., Northway, M., Ziemann, P. J., Canagaratna, M. R., Onasch, T. B., Alfarra, M. R., Prevot, A. S. H., Dommen, J., Duplissy, J., Metzger, A., Baltensperger, U., and Jimenez, J. L.: O/C and OM/OC ratios of primary, secondary, and ambient organic aerosols with high-resolution time-of-flight aerosol mass spectrometry, Environmental Science and Technology, 42, 4478-4485, 2008.

Aiken, A. C., Salcedo, D., Cubison, M. J., Huffman, J. A., DeCarlo, P. F., Ulbrich, I. M., Docherty, K. S., Sueper, D., Kimmel, J. R., Worsnop, D. R., Trimborn, A., Northway, M., Stone, E. A., Schauer, J. J., Volkamer, R., Fortner, E., De Foy, B., Wang, J., Laskin, A., Shutthanandan, V., Zheng, J., Zhang, R., Gaffney, J., Marley, N. A., Paredes-Miranda, G., Arnott, W. P., Molina, L. T., Sosa, G., and Jimenez, J. L.: Mexico City aerosol analysis during MILAGRO using high resolution aerosol mass spectrometry at the urban supersite (T0) - Part 1: Fine particle composition and organic source apportionment, Atmospheric Chemistry and Physics, 9, 6633-6653, 2009.

Allan, D., Williams, P. I., Morgan, W. T., Martin, C. L., Flynn, M. J., Lee, J., Nemitz, E., Phillips, G. J., Gallagher, M. W., and Coe, H.: Contributions from transport, solid fuel burning and cooking to primary organic aerosols in two UK cities, Atmospheric Chemistry and Physics, 10, 647-668, 2010.

Allan, J. D., Jimenez, J. L., Williams, P. I., Alfarra, M. R., Bower, K. N., Jayne, J. T., Coe, H., and Worsnop, D. R.: Quantitative sampling using an Aerodyne aerosol mass spectrometer: 1. Techniques of data interpretation and error analysis (vol 108, art no 4090, 2003), Journal of Geophysical Research-Atmospheres, 108, 1, 4283, 2003, doi:10.1029/2002JD002358.

Allan, J. D., Delia, A. E., Coe, H., Bower, K. N., Alfarra, M. R., Jimenez, J. L., Middlebrook, A. M., Drewnick, F., Onasch, T. B., Canagaratna, M. R., Jayne, J. T., and Worsnopf, D. R.: A generalised method for the extraction of chemically resolved mass spectra from aerodyne aerosol mass spectrometer data, Journal of Aerosol Science, 35, 909-922, 2004.

Anderson, J. O., Thundiyil, J. G., and Stolbach, A.: Clearing the Air: A Review of the Effects of Particulate Matter Air Pollution on Human Health, Journal of Medical Toxicology, 8, 166-175, 2012.

Ashbaugh, L. L., Malm, W. C., and Sadeh, W. Z.: A residence time probability analysis of sulfur concentrations at Grand-Canyon National Park, Atmospheric Environment, 19, 1263-1270, 1985.

Brook, R. D., Rajagopalan, S., Pope, C. A., Brook, J. R., Bhatnagar, A., Diez-Roux, A. V., Holguin, F., Hong, Y., Luepker, R. V., Mittleman, M. A., Peters, A., Siscovick, D., Smith, S. C., Whitsel, L., and Kaufman, J. D.: Particulate matter air pollution and cardiovascular disease: An update to the scientific statement from the american heart association, Circulation, 121, 2331-2378, 2010.

Brown, S. G., Lee, T., Norris, G. A., Roberts, P. T., Collett, J. L., Paatero, P., and Worsnop, D. R.: Receptor modeling of near-roadway aerosol mass spectrometer data in Las Vegas, Nevada, with EPA PMF, Atmospheric Chemistry and Physics, 12, 309-325, 10.5194/acp-12-309-2012, 2012.

Buset, K. C., Evans, G. J., Leaitch, W. R., Brook, J. R., and Toom-Sauntry, D.: Use of advanced receptor modelling for analysis of an intensive 5-week aerosol sampling campaign, Atmospheric Environment, 40, S482-S499, 2006.

Canagaratna, M. R., Jayne, J. T., Jimenez, J. L., Allan, J. D., Alfarra, M. R., Zhang, Q., Onasch, T. B., Drewnick, F., Coe, H., Middlebrook, A., Delia, A., Williams, L. R., Trimborn, A. M., Northway, M. J., DeCarlo, P. F., Kolb, C. E., Davidovits, P., and Worsnop, D. R.: Chemical and microphysical characterization of ambient aerosols with the aerodyne aerosol mass spectrometer, Mass Spectrometry Reviews, 26, 185-222, 2007a.

Canagaratna, M. R., Jayne, J. T., Jimenez, J. L., Allan, J. D., Alfarra, M. R., Zhang, Q., Onasch, T. B., Drewnick, F., Coe, H., Middlebrook, A., Delia, A., Williams, L. R., Trimborn, A. M., Northway, M. J., DeCarlo, P. F., Kolb, C. E., Davidovits, P., and Worsnop, D. R.: Chemical and microphysical characterization of ambient aerosols with the aerodyne aerosol mass spectrometer, Mass Spectrom. Rev., 26, 185–222, 2007b.

Chang, R. Y. W., Leck, C., Graus, M., Müller, M., Paatero, J., Burkhart, J. F., Stohl, A., Orr, L. H., Hayden, K., Li, S. M., Hansel, A., Tjernström, M., Leaitch, W. R., and Abbatt, J. P. D.: Aerosol composition and sources in the central Arctic Ocean during ASCOS, Atmospheric Chemistry and Physics, 11, 10619-10636, 2011.

Chirico, R., Prevot, A. S. H., DeCarlo, P. F., Heringa, M. F., Richter, R., Weingartner, E., and Baltensperger, U.: Aerosol and trace gas vehicle emission factors measured in a tunnel using an Aerosol Mass Spectrometer and other on-line instrumentation, Atmospheric Environment, 45, 2182-2192, 10.1016/j.atmosenv.2011.01.069, 2011.

Crippa, M., DeCarlo, P. F., Slowik, J. G., Mohr, C., Heringa, M. F., Chirico, R., Poulain, L., Freutel, F., Sciare, J., Cozic, J., Di Marco, C. F., Elsasser, M., José, N., Marchand, N., Abidi, E., Wiedensohler, A., Drewnick, F., Schneider, J., Borrmann, S., Nemitz, E., Zimmermann, R., Jaffrezo, J.-L., Prévôt, A. S. H., and Baltensperger, U.: Wintertime aerosol chemical composition and source apportionment of the organic fraction in the metropolitan area of Paris, Atmos. Chem. Phys., 13, 961-981, 2013a.

Crippa, M., El Haddad, I., Slowik, J. G., Decarlo, P. F., Mohr, C., Heringa, M. F., Chirico, R., Marchand, N., Sciare, J., Baltensperger, U., and Prévôt, A. S. H.: Identification of marine and continental aerosol sources in Paris using high resolution aerosol mass spectrometry, Journal of Geophysical Research D: Atmospheres, 118, 1950-1963, 2013b.

Docherty, K. S., Aiken, A. C., Huffman, J. A., Ulbrich, I. M., DeCarlo, P. F., Sueper, D., Worsnop, D. R., Snyder, D. C., Peltier, R. E., Weber, R. J., Grover, B. D., Eatough, D. J., Williams, B. J., Goldstein, A. H., Ziemann, P. J., and Jimenez, J. L.: The 2005 Study of Organic Aerosols at Riverside (SOAR-1): instrumental intercomparisons and fine particle composition, Atmospheric Chemistry and Physics, 11, 12387-12420, 10.5194/acp-11-12387-2011, 2011.

Drewnick, F., Hings, S. S., Curtius, J., Eerdekens, G., and Williams, J.: Measurement of fine particulate and gas-phase species during the New Year's fireworks 2005 in Mainz, Germany, Atmospheric Environment, 40, 4316-4327, 2006.

Environment Canada: National Pollutant Release Inventory, 2013, downloadable at http://www.ec.gc.ca/inrp-npri/, accessed December 2013.

Ge, X., Wexler, A. S., and Clegg, S. L.: Atmospheric amines - Part I. A review, Atmospheric Environment, 45, 524-546, 2011.

Godri, K. J., Evans, G. J., Slowik, J., Knox, A., Abbatt, J., Brook, J., Dann, T., and Dabek-Zlotorzynska, E.: Evaluation and application of a semi-continuous chemical characterization system for water soluble inorganic PM2.5 and associated precursor gases, Atmospheric Measurement Techniques, 2, 65-80, 2009.

Gordon, G. E.: Receptor Models, Environmental Science & Technology, 14, 792-800, 1980.

Greim, H., Bury, D., Klimisch, H. J., Oeben-Negele, M., and Ziegler-Skylakakis, K.: Toxicity of aliphatic amines: Structure-activity relationship, Chemosphere, 36, 271-295, 1998.

Hildebrandt, L., Kostenidou, E., Lanz, V. A., Prevot, A. S. H., Baltensperger, U., Mihalopoulos, N., Laaksonen, A., Donahue, N. M., and Pandis, S. N.: Sources and atmospheric processing of organic aerosol in the Mediterranean: Insights from aerosol mass spectrometer factor analysis, Atmospheric Chemistry and Physics, 11, 12499-12515, 2011.

Hogrefe, O., Drewnick, F., Lala, G. G., Schwab, J. J., and Demerjian, K. L.: Development, operation and applications of an aerosol generation, calibration and research facility, Aerosol Science and Technology, 38, 196-214, 2004.

Hopke, P. K.: Recent developments in receptor modeling, Journal of Chemometrics, 17, 255-265, 2003.

Huffman, J. A., Docherty, K. S., Aiken, A. C., Cubison, M. J., Ulbrich, I. M., Decarlo, P. F., Sueper, D., Jayne, J. T., Worsnop, D. R., Ziemann, P. J., and Jimenez, J. L.: Chemically-resolved aerosol volatility measurements from two megacity field studies, Atmospheric Chemistry and Physics, 9, 7161-7182, 2009.

IPCC: Intergovernmental Panel on Climate Change, Fifth Assessment Report, 2013, downloadable at http://www.ipcc.ch/, accessed December 2013.

Jayne, J. T., Leard, D. C., Zhang, X. F., Davidovits, P., Smith, K. A., Kolb, C. E., and Worsnop, D. R., Development of an aerosol mass spectrometer for size and composition analysis of submicron particles, Aerosol Sci. Tech., 33, 49–70, 2000.

Jeong, C.-H., McGuire, M. L., Herod, D., Dann, T., Dabek-Zlotorzynska, E., Wang, D., Ding, L., Celo, V., Mathieu, D., and Evans, G. J.: Receptor Model Based Identification of the Sources of PM2.5 in Canadian Cities, Atmospheric Pollution Research, 2, 158-171, 2011.

Jimenez, J. L., Canagaratna, M. R., Donahue, N. M., Prevot, A. S. H., Zhang, Q., Kroll, J. H., DeCarlo, P. F., Allan, J. D., Coe, H., Ng, N. L., Aiken, A. C., Docherty, K. S., Ulbrich, I. M., Grieshop, A. P., Robinson, A. L., Duplissy, J., Smith, J. D., Wilson, K. R., Lanz, V. A., Hueglin, C., Sun, Y. L., Tian, J., Laaksonen, A., Raatikainen, T., Rautiainen, J., Vaattovaara, P., Ehn, M., Kulmala, M., Tomlinson, J. M., Collins, D. R., Cubison, M. J., Dunlea, E. J., Huffman, J. A., Onasch, T. B., Alfarra, M. R., Williams, P. I., Bower, K., Kondo, Y., Schneider, J., Drewnick, F., Borrmann, S., Weimer, S., Demerjian, K., Salcedo, D., Cottrell, L., Griffin, R., Takami, A., Miyoshi, T., Hatakeyama, S., Shimono, A., Sun, J. Y., Zhang, Y. M., Dzepina, K., Kimmel, J. R., Sueper, D., Jayne, J. T., Herndon, S. C., Trimborn, A. M., Williams, L. R., Wood, E. C., Middlebrook, A. M., Kolb, C. E., Baltensperger, U., and Worsnop, D. R.: Evolution of organic aerosols in the atmosphere, Science, 326, 1525-1529, 2009.

Langley, L., Leaitch, W. R., Lohmann, U., Shantz, N. C., and Worsnop, D. R.: Contributions from DMS and ship emissions to CCN observed over the summertime North Pacific, Atmospheric Chemistry and Physics, 10, 1287-1314, 2010.

Lanz, V. A., Alfarra, M. R., Baltensperger, U., Buchmann, B., Hueglin, C., and Prevot, A. S. H.: Source apportionment of submicron organic aerosols at an urban site by factor analytical modelling of aerosol mass spectra, Atmospheric Chemistry and Physics, 7, 1503-1522, 2007.

Lanz, V. A., Alfarra, M. R., Baltensperger, U., Buchmann, B., Hueglin, C., Szidat, S., Wehrli, M. N., Wacker, L., Weimer, S., Caseiro, A., Puxbaum, H., and Prevot, A. S. H.: Source attribution of submicron organic aerosols during wintertime inversions by advanced factor analysis of aerosol mass spectra, Environmental Science and Technology, 42, 214-220, 2008.

Li, Y. Q., Schwab, J. J., and Demerjian, K. L.: Measurements of ambient ammonia using a tunable diode laser absorption spectrometer: Characteristics of ambient ammonia emissions in an urban area of New York City, Journal of Geophysical Research-Atmospheres, 111, 11, D10s02, 2006, doi:10.1029/2005JD006275.

Liggio, J., Li, S. M., Vlasenko, A., Stroud, C., and Makar, P.: Depression of ammonia uptake to sulfuric acid aerosols by competing uptake of ambient organic gases, Environmental Science and Technology, 45, 2790-2796, 2011.

Liggio, J., and Li, S. M.: A new source of oxygenated organic aerosol and oligomers, Atmospheric Chemistry and Physics, 13, 2989-3002, 2013.

Malloy, Q. G. J., Qi, L., Warren, B., Cocker, D. R., Erupe, M. E., and Silva, P. J.: Secondary organic aerosol formation from primary aliphatic amines with NO3 radical, Atmospheric Chemistry and Physics, 9, 2051-2060, 2009.

McGuire, M. L., Jeong, C. H., Slowik, J. G., Chang, R. Y. W., Corbin, J. C., Lu, G., Mihele, C., Rehbein, P. J. G., Sills, D. M. L., Abbatt, J. P. D., Brook, J. R., and Evans, G. J.: Elucidating determinants of aerosol composition through particle-type-based receptor modeling, Atmospheric Chemistry and Physics, 11, 8133-8155, 10.5194/acp-11-8133-2011, 2011.

McLafferty, F. W., and Tureček, F.: Interpretation of mass spectra, 4th ed., University Science Books, Sausalito, Calif., xviii, 371 p. pp., 1993.

Middlebrook, A. M., Bahreini, R., Jimenez, J. L., and Canagaratna, M. R.: Evaluation of composition-dependent collection efficiencies for the Aerodyne aerosol mass spectrometer using field data, Aerosol Science and Technology, 46, 258-271, 2012.

Moffet, R. C., de Foy, B., Molina, L. T., Molina, M. J., and Prather, K. A.: Measurement of ambient aerosols in northern Mexico City by single particle mass spectrometry, Atmospheric Chemistry and Physics, 8, 4499-4516, 2008a.

Moffet, R. C., Desyaterik, Y., Hopkins, R. J., Tivanski, A. V., Gilles, M. K., Wang, Y., Shutthanandan, V., Molina, L. T., Abraham, R. G., Johnson, K. S., Mugica, V., Molina, M. J., Laskin, A., and Prather, K. A.: Characterization of aerosols containing Zn, Pb, and Cl from an industrial region of Mexico City, Environmental Science & Technology, 42, 7091-7097, doi: 10.1021/es7030483, 2008b.

Mohr, C., DeCarlo, P. F., Heringa, M. F., Chirico, R., Slowik, J. G., Richter, R., Reche, C., Alastuey, A., Querol, X., Seco, R., Peñuelas, J., Jiménez, J. L., Crippa, M., Zimmermann, R., Baltensperger, U., and Prévôt, A. S. H.: Identification and quantification of organic aerosol from cooking and other sources in Barcelona using aerosol mass spectrometer data, Atmospheric Chemistry and Physics, 12, 1649-1665, 2012.

Murphy, S. M., Sorooshian, A., Kroll, J. H., Ng, N. L., Chhabra, P., Tong, C., Surratt, J. D., Knipping, E., Flagan, R. C., and Seinfeld, J. H.: Secondary aerosol formation from atmospheric reactions of aliphatic amines, Atmospheric Chemistry and Physics, 7, 2313-2337, 2007.

Ng, N. L., Canagaratna, M. R., Zhang, Q., Jimenez, J. L., Tian, J., Ulbrich, I. M., Kroll, J. H., Docherty, K. S., Chhabra, P. S., Bahreini, R., Murphy, S. M., Seinfeld, J. H., Hildebrandt, L., Donahue, N. M., Decarlo, P. F., Lanz, V. A., Prévôt, A. S. H., Dinar, E., Rudich, Y., and Worsnop, D. R.: Organic aerosol components observed in Northern Hemispheric datasets from Aerosol Mass Spectrometry, Atmospheric Chemistry and Physics, 10, 4625-4641, 2010.

Norris, G., Vedantham, R., Duvall, R., Wade, K., Brown, S., Prouty, J., Bai, S., and DeWinter, J.: EPA Positive Matrix Factorization 4.1 Fundamentals & User Guide, EPA, Research Triangle Park, North Carolina, 2010.

Paatero, P., and Tapper, U.: Analysis of Different Modes of Factor-Analysis as Least-Squares Fit Problems, Chemometrics and Intelligent Laboratory Systems, 18, 183-194, 1993.

Paatero, P., and Tapper, U.: Positive Matrix Factorization - A Nonnegative Factor Model With Optimal Utilization of Error-Estimates of Data Values, Environmetrics, 5, 111-126, 1994.

Paatero, P.: Least squares formulation of robust non-negative factor analysis, Chemometrics and Intelligent Laboratory Systems, 37, 23-35, 1997.

Perron, N., Sandradewi, J., Alfarra, M. R., Lienemann, P., Gehrig, R., Kasper-Giebl, A., Lanz, V. A., Szidat, S., Ruff, M., Fahrni, S., Wacker, L., Baltensperger, U., and Prévôt, A. S. H.: Composition and sources of particulate matter in an industrialised Alpine valley, Atmospheric Chemistry and Physics Discussions, 10, 9391-9430, 2010.

Pio, C. A., and Harrison, R. M.: The equilibrium of ammonium chloride aerosol with gaseous hydrochloric acid and ammonia under tropospheric conditions, Atmospheric Environment, 21, 1243-1246, 1987a.

Pio, C. A., and Harrison, R. M.: Vapour pressure of ammonium chloride aerosol: Effect of temperature and humidity, Atmospheric Environment, 21, 2711-2715, 1987b.

Pope, C. A., and Dockery, D. W.: Health effects of fine particulate air pollution: Lines that connect, Journal of the Air & Waste Management Association, 56, 709-742, 2006.

Pratt, K. A., Hatch, L. E., and Prather, K. A.: Seasonal volatility dependence of ambient particle phase amines, Environmental Science and Technology, 43, 5276-5281, 2009.

Rehbein, P. J. G., Jeong, C.-H., McGuire, M. L., Yao, X., Corbin, J., and Evans, G. J.: Cloud and Fog Processing Enhanced Gas-to-Particle Partitioning of Trimethylamine, Environmental Science and Technology, 45, 4346-4352, 2011.

Richard, A., Gianini, M. F. D., Mohr, C., Furger, M., Bukowiecki, N., Minguillón, M. C., Lienemann, P., Flechsig, U., Appel, K., Decarlo, P. F., Heringa, M. F., Chirico, R., Baltensperger, U., and Prévôt, A. S. H.: Source apportionment of size and time resolved trace elements and organic aerosols from an urban courtyard site in Switzerland, Atmospheric Chemistry and Physics, 11, 8945-8963, 2011.

Salcedo, D., Onasch, T. B., Dzepina, K., Canagaratna, M. R., Zhang, Q., Huffman, J. A., DeCarlo, P. F., Jayne, J. T., Mortimer, P., Worsnop, D. R., Kolb, C. E., Johnson, K. S., Zuberi, B., Marr, L. C., Volkamer, R., Molina, L. T., Molina, M. J., Cardenas, B., Bernabe, R. M., Marquez, C., Gaffney, J. S., Marley, N. A., Laskin, A., Shutthanandan, V., Xie, Y., Brune, W., Lesher, R., Shirley, T., and Jimenez, J. L.: Characterization of ambient aerosols in

Mexico City during the MCMA-2003 campaign with Aerosol Mass Spectrometry: results from the CENICA Supersite, Atmospheric Chemistry and Physics, 6, 925-946, 2006.

Silva, P. J., Erupe, M. E., Price, D., Elias, J., Malloy, Q. G. J., Li, Q., Warren, B., and Cocker Iii, D. R.: Trimethylamine as precursor to secondary organic aerosol formation via nitrate radical reaction in the atmosphere, Environmental Science and Technology, 42, 4689-4696, 2008.

Slowik, J. G., Vlasenko, A., McGuire, M., Evans, G. J., and Abbatt, J. P. D.: Simultaneous factor analysis of organic particle and gas mass spectra: AMS and PTR-MS measurements at an urban site, Atmospheric Chemistry and Physics Discussions, Submitted, 2009.

Slowik, J. G., Vlasenko, A., McGuire, M., Evans, G. J., and Abbatt, J. P. D.: Simultaneous factor analysis of organic particle and gas mass spectra: AMS and PTR-MS measurements at an urban site, Atmospheric Chemistry and Physics, 10, 1969-1988, 2010.

Stein, S. E.: "Mass Spectra", NIST Chemistry WebBook, NIST Standard Reference Database Number 69, National Institute of Standards and Technology, Gaithersburg MD, 20899, 2013.

Sun, Y. L., Zhang, Q., Schwab, J. J., Demerjian, K. L., Chen, W. N., Bae, M. S., Hung, H. M., Hogrefe, O., Frank, B., Rattigan, O. V., and Lin, Y. C.: Characterization of the sources and processes of organic and inorganic aerosols in New York city with a high resolution time-of-flight aerosol mass spectrometer, Atmospheric Chemistry and Physics, 11, 1581-1602, 2011.

Sun, Y. L., Zhang, Q., Schwab, J. J., Yang, T., Ng, N. L., and Demerjian, K. L.: Factor analysis of combined organic and inorganic aerosol mass spectra from high resolution aerosol mass spectrometer measurements, Atmospheric Chemistry and Physics, 12, 8537-8551, 2012.

Tan, P. V., Evans, G. J., Tsai, J., Owega, S., Fila, S., Malpica, O., and Brook, J. R.: On-line analysis of urban particulate matter focusing on elevated wintertime aerosol concentrations, Environmental Science and Technology, 36, 3512-3518, 2002.

Ulbrich, I. M., Canagaratna, M. R., Zhang, Q., Worsnop, D. R., and Jimenez, J. L.: Interpretation of organic components from positive matrix factorization of aerosol mass spectrometric data, Atmospheric Chemistry and Physics Discussions, 8, 6729-6791, 2008.

Ulbrich, I. M., Canagaratna, M. R., Zhang, Q., Worsnop, D. R., and Jimenez, J. L.: Interpretation of Organic Components from Positive Matrix Factorization of Aerosol Mass Spectrometric Data, Atmospheric Chemistry and Physics, 9, 2891-2918, 2009.

US EPA: National Emission Inventory (NEI) 2013: Inventory Data: Point Sector Data - ALLNEI HAP Annual, Research Triangle Park, North Carolina, 2013.

US EPA: Toxics Release Inventory, Washington, DC, 2013.

Vlasenko, A., Slowik, J. G., Bottenheim, J. W., Brickell, P. C., Chang, R. Y. W., Maedonald, A. M., Shantz, N. C., Sjostedt, S. J., Wiebe, H. A., Leaitch, W. R., and Abbatt, J. P. D.: Measurements of VOCs by proton transfer reaction mass spectrometry at a rural Ontario site: Sources and correlation to aerosol composition, J. Geophys. Res., 114, D21305, doi:10.1029/2009JD012025.

Watson, J. G.: Visibility: Science and Regulation, Journal of the Air and Waste Management Association, 52, 628-713, 2002.

Watson, J. G., Chen, L. W. A., Chow, J. C., Doraiswamy, P., and Lowenthal, D. H.: Source apportionment: Findings from the U.S. supersites program, Journal of the Air and Waste Management Association, 58, 265-288, 2008.

Zhang, Q., Alfarra, M. R., Worsnop, D. R., Allan, J. D., Coe, H., Canagaratna, M. R., and Jimenez, J. L.: Deconvolution and quantification of hydrocarbon-like and oxygenated organic aerosols based on aerosol mass spectrometry, Environmental Science & Technology, 39, 4938-4952, 2005.

Zhang, Q., Jimenez, J. L., Canagaratna, M. R., Allan, J. D., Coe, H., Ulbrich, I., Alfarra, M. R., Takami, A., Middlebrook, A. M., Sun, Y. L., Dzepina, K., Dunlea, E., Docherty, K., DeCarlo, P. F., Salcedo, D., Onasch, T., Jayne, J. T., Miyoshi, T., Shimono, A., Hatakeyama, S., Takegawa, N., Kondo, Y., Schneider, J., Drewnick, F., Borrmann, S., Weimer, S., Demerjian, K., Williams, P., Bower, K., Bahreini, R., Cottrell, L., Griffin, R. J., Rautiainen, J., Sun, J. Y., Zhang, Y. M., and Worsnop, D. R.: Ubiquity and dominance of oxygenated species in organic aerosols in anthropogenically-influenced Northern Hemisphere midlatitudes, Geophysical Research Letters, 34, 6, L13801, doi:10.1029/2007GL029979, 2007.

Zhang, Q., Jimenez, J. L., Canagaratna, M. R., Ulbrich, I. M., Ng, N. L., Worsnop, D. R., and Sun, Y.: Understanding atmospheric organic aerosols via factor analysis of aerosol mass spectrometry: A review, Analytical and Bioanalytical Chemistry, 401, 3045-3067, 2011.

Zorn, S. R., Drewnick, F., Schott, M., Hoffmann, T., and Borrmann, S.: Characterization of the South Atlantic marine boundary layer aerosol using an aerodyne aerosol mass spectrometer, Atmospheric Chemistry and Physics, 8, 4711-4728, 2008.

Table Captions

Table 1: Descriptive statistics for AMS measured non-refractory sub-micron PM species, pre- and post-PMF analysis (μg m^{-3}).

Table 2: Chemical composition of the six factors from the $PMF_{Full\ MS}$ analysis, extent of neutralization, and F44 for each factor's organic fraction.

Figure Captions

Figure 1: The location of the sampling site (MicMac Park) in Windsor, Ontario relative to major industrial sources, namely coal fired power plants, steel mills, and potential large amine sources. It can be seen that the measurement site was located close to the largest international border crossing between the US and Canada (Huron Church road and the Ambassador Bridge).

Figure 2: Meteorological conditions and $PM_{2.5}$ mass concentration from the CRUISER TEOM for the MicMac Park winter campaign.

Figure 3: Time series of AMS-measured non-refractory sub-micron PM species.

Figure 4: Time series of the factors from the six factor solution from $PMF_{Full\ MS}$ analysis. The solid line represents FPeak = 0, and the range of uncertainties through FPeak analysis (-10 and +10) is shown in the shaded regions.

Figure 5: Mass spectra of factors from the six factor solution from $PMF_{Full\ MS}$ analysis. Bars represent the central, chosen rotation, and dots show the range in mass spectral variation from FPeak rotations (-10 and 10).

Figure 6: Mass spectra of the organic fraction of the factors from the six factor solution from $PMF_{Full\ MS}$ analysis. The Amine factor is not shown due to insufficient information regarding the chemical nature of the Amine factor. Bars represent the central, chosen rotation, and dots show the range in mass spectral variation from FPeak rotations (-10 and 10).

Figure 7: Chemical composition by factor and species components of the six PMF factors from the $PMF_{Full\ MS}$ analysis.

Figure 8: Conditional probability function (CPF) plots for the six factors from the six factor solution of the $PMF_{Full\ MS}$ analysis, along with a wind rose plot (wind speed in m s^{-1}). The strongest wind dependence is observed for the Amine and Sulphate-OA factors, which show strong, yet slightly different directional associations to the southwest.

Figure 9: Potential source contribution function (PSCF) plot for the Sulphate-OA (a) and the Nitrate-OA factor (b) from the $PMF_{Full\ MS}$ analysis. Both factors showed regional source influences, with the Sulphate-OA factor showing more prominent, distant influences to the south and southwest. The Nitrate-OA factor showed the most prominent influences to the southwest, over Indiana and Illinois.

Figure 10: Particulate sulphate concentration (SO_4^{2-}) vs. $SO_{2(g)}$ concentration, and fraction of SO_4^{2-} / Total S (Total S = SO_4^{2-} + SO_2) (a). Due to the winter conditions,

the fractional contribution of pSO_4^{2-} to total S was typically very low. Shown in (b) are the averaged particle size distributions of AMS SO_4^{2-} over the entire campaign, as well as during the extreme SO_4^{2-} spikes. Particulate SO_4^{2-} measured during the spikes appeared highly local due to their significantly smaller modal diameter.

Figure 11: Boxplots of diurnal trends for the Sulphate-OA (a), Nitrate-OA (b), HOA (c), and OOA factors (d), from the $PMF_{Full\ MS}$ analysis, along with temperature (e). Boxes indicate interquartile ranges, horizontal lines indicate median hourly values, cross markers indicate hourly means, and whiskers represent the 5^{th} and 95^{th} percentiles. The HOA factor demonstrated a strong diurnal trend consistent with traffic patterns, while the OOA factor demonstrated a trend more consistent with daytime lows and overnight highs. The Nitrate-OA factor showed a minor diurnal trend indicative of more regional contributions as compared to OOA, while the Sulphate-OA factor showed minimal diurnal trend.

Figure 12: Comparison of factor profiles from the $PMF_{Org\ MS}$ analysis to comparable factors found by PMF of the full mass spectra (a, b, and c). The factors are normalized to the total organic fraction signal, except for the Amine factor which is normalized to the total factor signal. Only minor differences in mass spectra are noted for the HOA factor. The most significant difference for the Amine factor is represented by the addition of the *m/z* 30 peak, and for the OOA factor with the difference in magnitude of the *m/z* 44 peak. Dots show the range in mass spectral variation from FPeak rotations (-10 and 10). Also shown in (d) is the average factor composition of organics for both the PMF of the full mass spectrum and of the organics only.

Figure 13: Scatter plots Amine (a), HOA (b), and OOA (c and d) factors comparing their mass derived from $PMF_{Full\ MS}$ vs. $PMF_{Org\ MS}$ analyses. One observation (01/31/2005 21:00) was removed from the HOA comparison to enhance the fit of the trendline.

Table 1: Descriptive statistics for AMS measured non-refractory sub-micron PM species, pre- and post-PMF analysis ($\mu g\ m^{-3}$).

	Org		NH_4^+		NO_3^-		SO_4^{2-}		Cl^-		Total	
	Pre	Post	Pre	Post	Pre	Post	Pre	Post	Pre	Post	Pre	Post
Mean	2.73	2.45	1.13	1.15	2.28	2.20	1.18	1.13	0.12	0.12	7.45	7.10
1σ	2.41	2.17	1.01	1.04	2.58	2.53	0.97	0.91	0.18	0.17	6.30	6.12
Min	0.29	0.00	0.00	0.00	0.01	0.00	0.03	0.00	0.00	0.00	0.58	0.00
Max	28.08	24.61	5.80	6.22	12.61	12.56	9.09	7.24	3.14	2.79	43.79	41.15

Table 2: Chemical composition of the six factors from the $PMF_{Full\ MS}$ analysis, extent of neutralization, and F44 for each factor's organic fraction.

PMF Factor	Sub-micron PM Mass ($\mu g\ m^{-3}$)	(%)	AMS Species (factor mass fractional contribution) SO_4^{2-}	Org	NO_3^-	NH_4^+	Cl^-	$Neut_{Ext}$	F44
Sulphate-OA	1.81	25	0.49	0.21	0.09	0.21	0.01	0.99	0.15
Nitrate-OA	3.19	45	0.06	0.16	0.58	0.20	0.00	1.04	0.12
Chloride	0.34	5	0.18	0.13	0.13	0.27	0.28	1.09	0.03
HOA	0.94	13	0.01	0.85	0.09	0.05	0.00	1.62	0.01
OOA	0.78	11	0.00	0.93	0.07	0.00	0.00	-	0.09
Amine	0.07	1	-	-	0.38	-	-	-	-

Figure 1: The location of the sampling site (MicMac Park) in Windsor, Ontario relative to major industrial sources, namely coal fired power plants, steel mills, and potential large amine sources. It can be seen that the measurement site was located close to the largest international border crossing between the US and Canada (Huron Church road and the Ambassador Bridge).

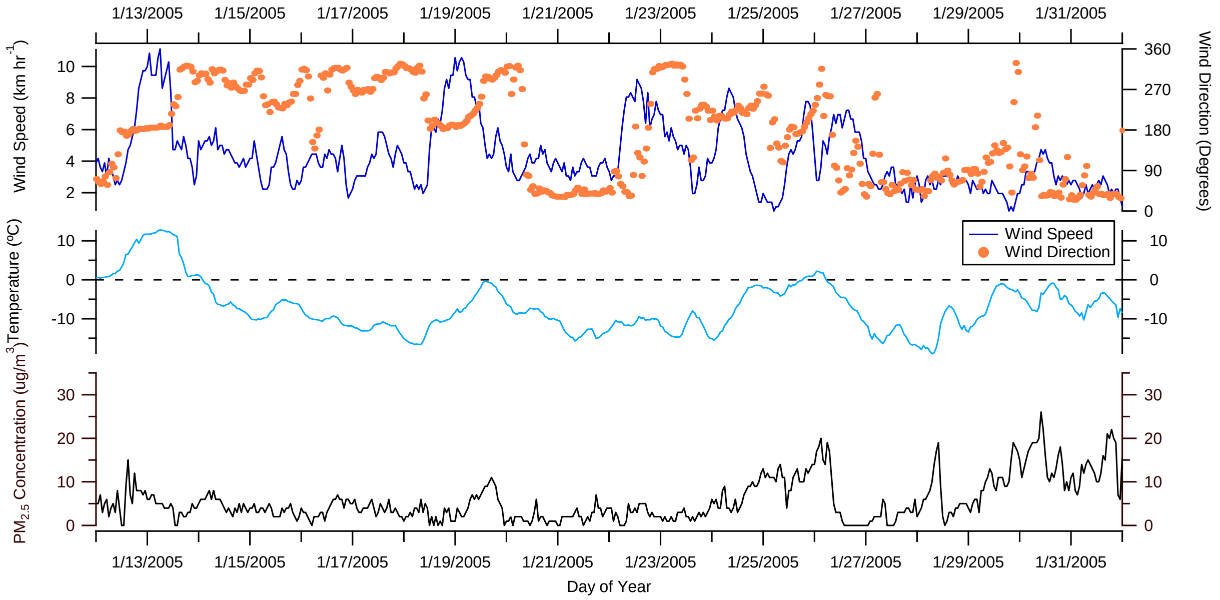

Figure 2: Meteorological conditions and $PM_{2.5}$ mass concentration from the CRUISER TEOM for the MicMac Park winter campaign.

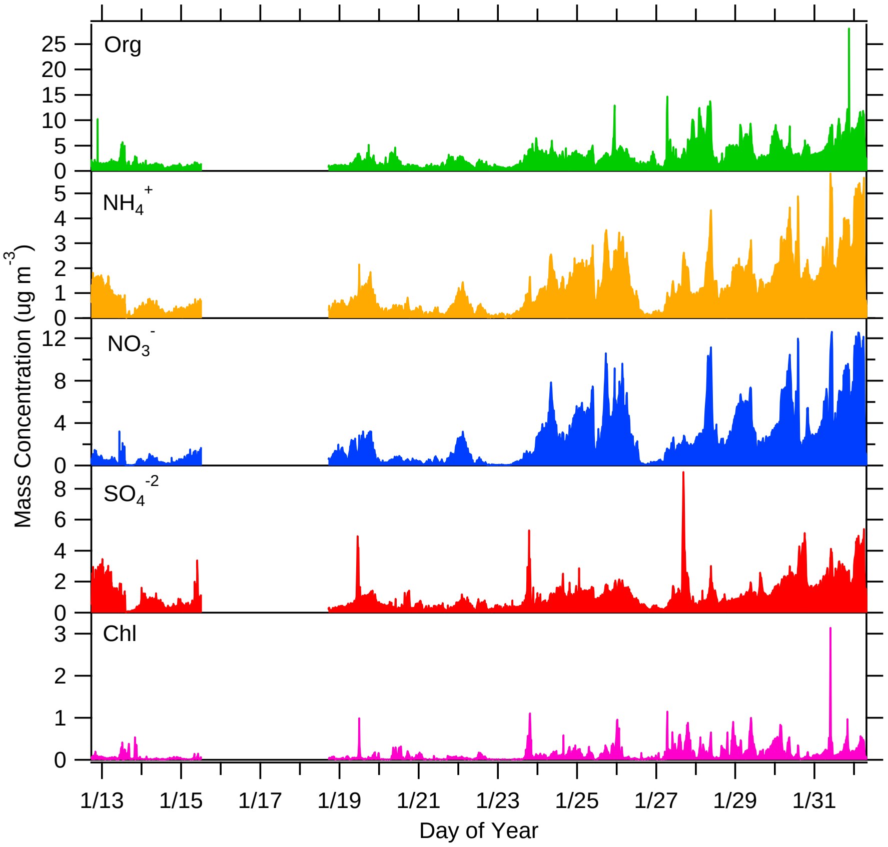

Figure 3: Time series of AMS-measured non-refractory sub-micron PM species.

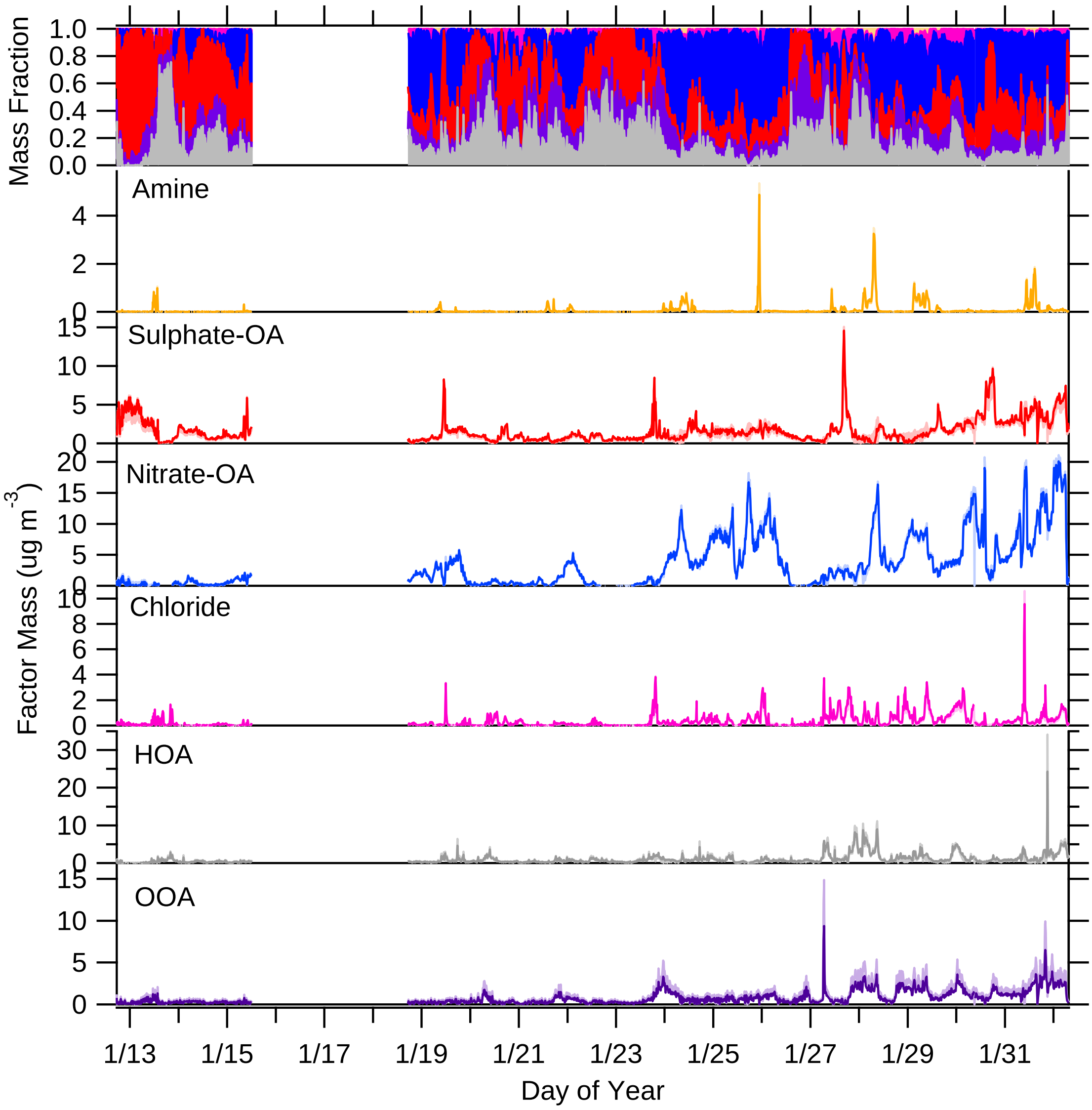

Figure 4: Time series of the factors from the six factor solution from $PMF_{Full\ MS}$ analysis. The solid line represents FPeak = 0, and the range of uncertainties through FPeak analysis (-10 and +10) is shown in the shaded regions.

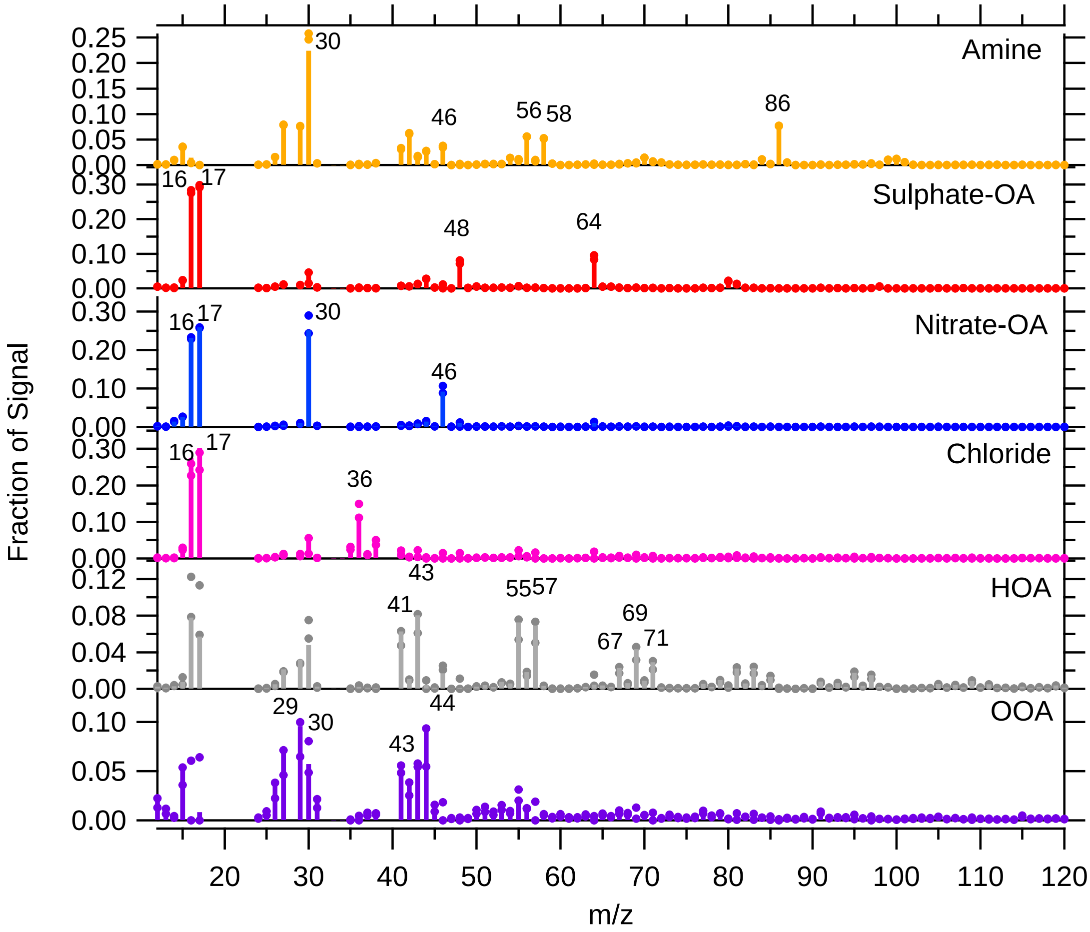

Figure 5: Mass spectra of factors from the six factor solution from $PMF_{Full\ MS}$ analysis. Bars represent the central, chosen rotation, and dots show the range in mass spectral variation from FPeak rotations (-10 and 10).

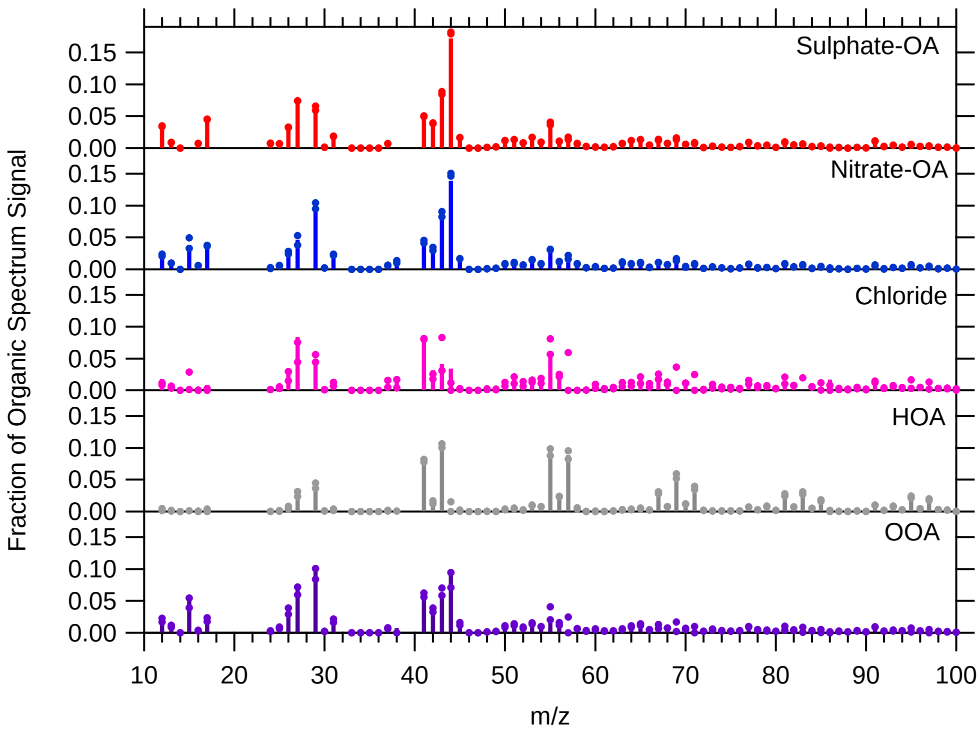

Figure 6: Mass spectra of the organic fraction of the factors from the six factor solution from $PMF_{Full\ MS}$ analysis. The Amine factor is not shown due to insufficient information regarding the chemical nature of the Amine factor. Bars represent the central, chosen rotation, and dots show the range in mass spectral variation from FPeak rotations (-10 and 10).

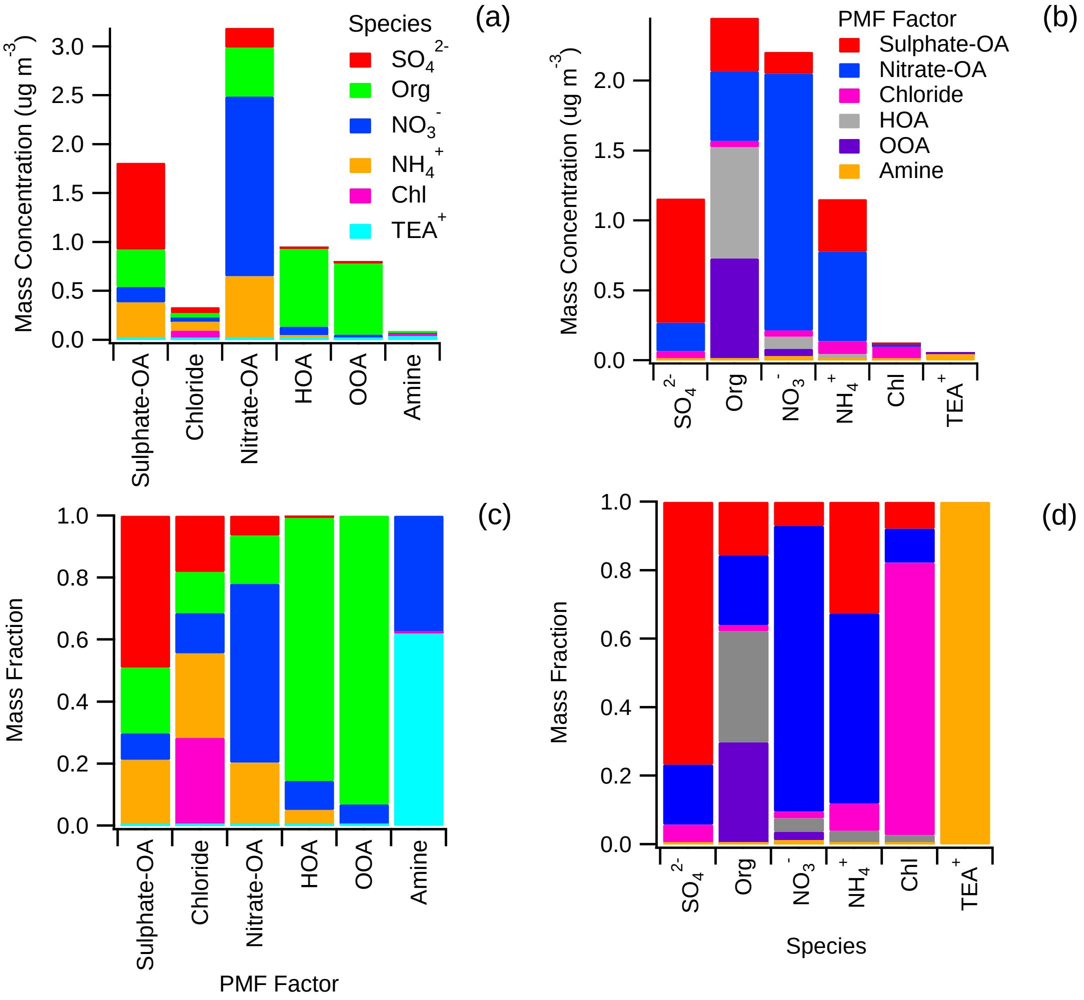

Figure 7: Chemical composition by factor and species components of the six PMF factors from the $PMF_{Full\ MS}$ analysis.

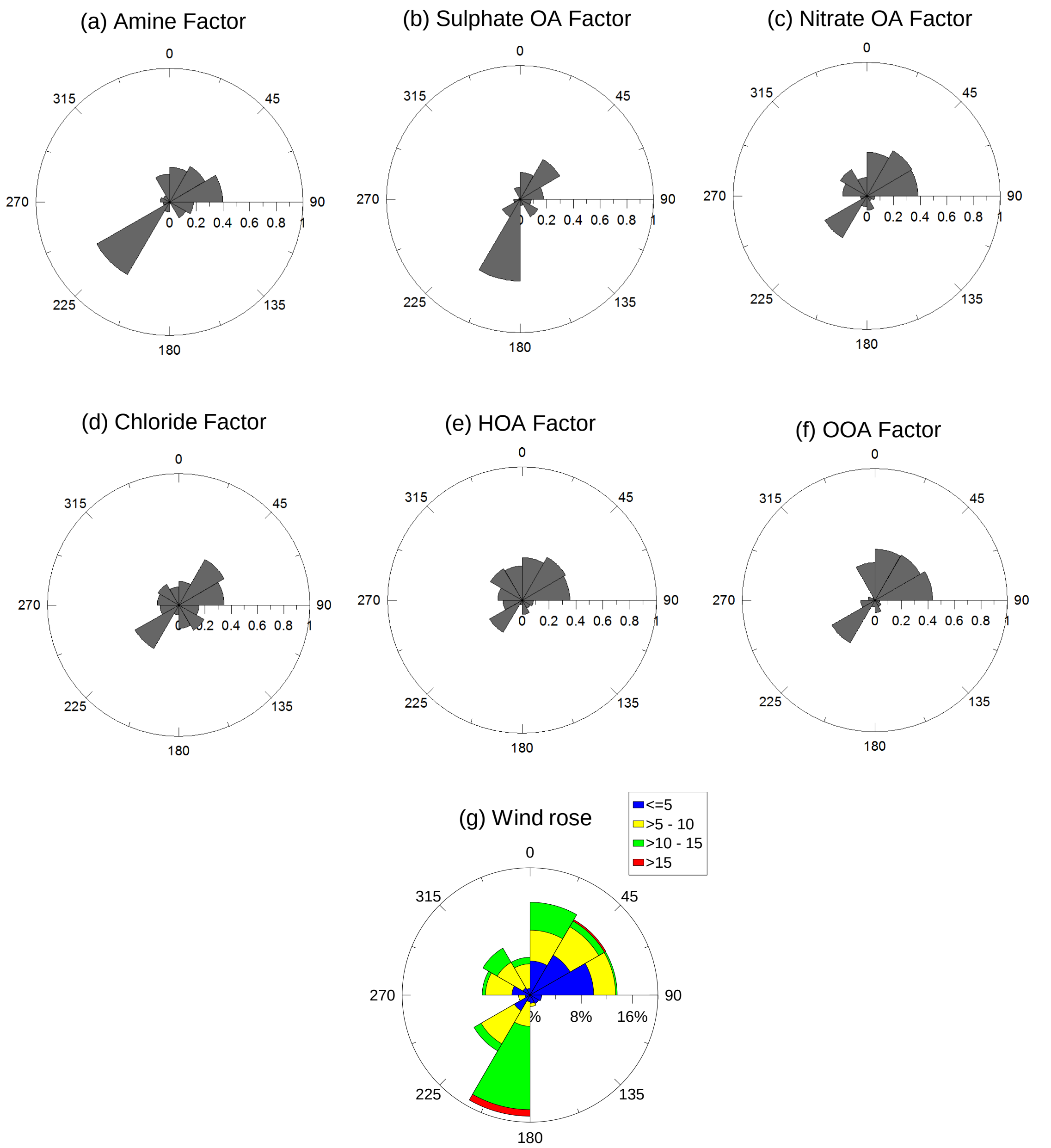

Figure 8: Conditional probability function (CPF) plots for the six factors from the six factor solution of the $PMF_{Full\ MS}$ analysis, along with a wind rose plot (wind speed in m s^{-1}). The strongest wind dependence is observed for the Amine and Sulphate-OA factors, which show strong, yet slightly different directional associations to the southwest.

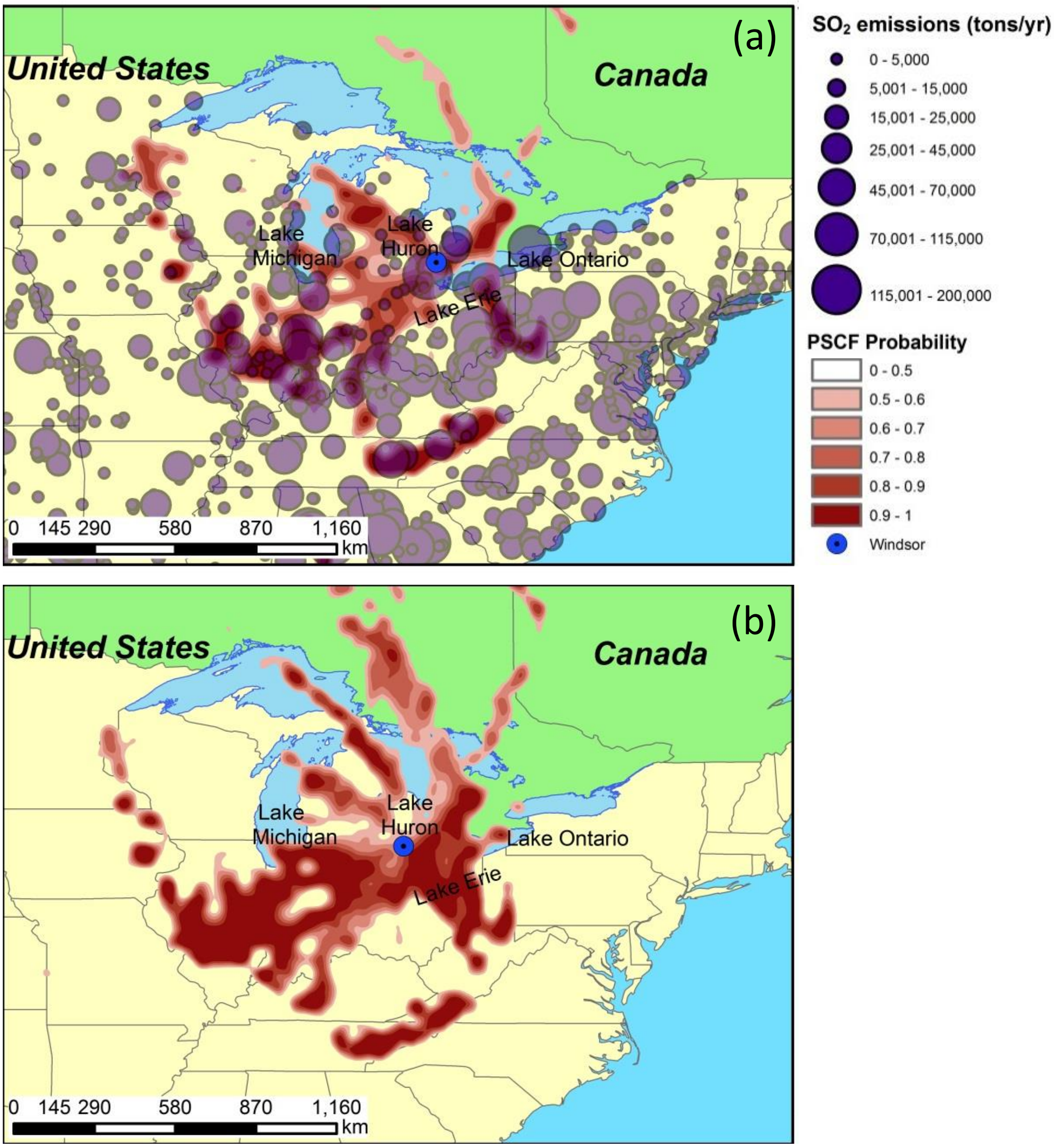

Figure 9: Potential source contribution function (PSCF) plot for the Sulphate-OA (a) and the Nitrate-OA factor (b) from the $PMF_{Full\ MS}$ analysis. Both factors showed regional source influences, with the Sulphate-OA factor showing more prominent, distant influences to the south and southwest. The Nitrate-OA factor showed the most prominent influences to the southwest, over Indiana and Illinois. SO_2 emissions represent emissions from major coal powered energy generating facilities.

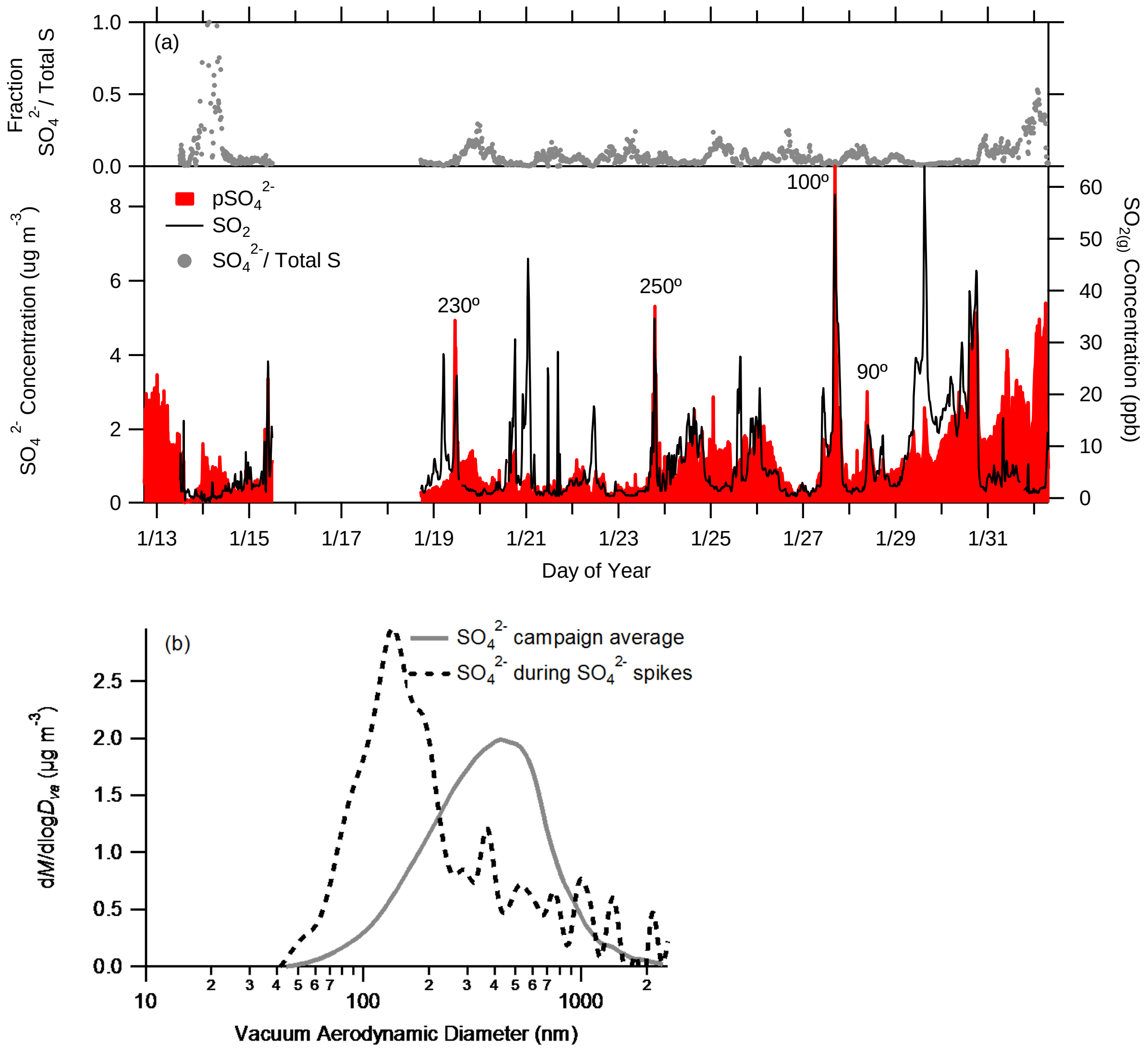

Figure 10: Particulate sulphate concentration (SO_4^{2-}) vs. $SO_{2(g)}$ concentration, and fraction of SO_4^{2-} / Total S (Total S = SO_4^{2-} + SO_2) (a). Due to the winter conditions, the fractional contribution of pSO_4^{2-} to total S was typically very low. Shown in (b) are the averaged particle size distributions of AMS SO_4^{2-} over the entire campaign, as well as during the extreme SO_4^{2-} spikes. Particulate SO_4^{2-} measured during the spikes appeared highly local due to their significantly smaller modal diameter.

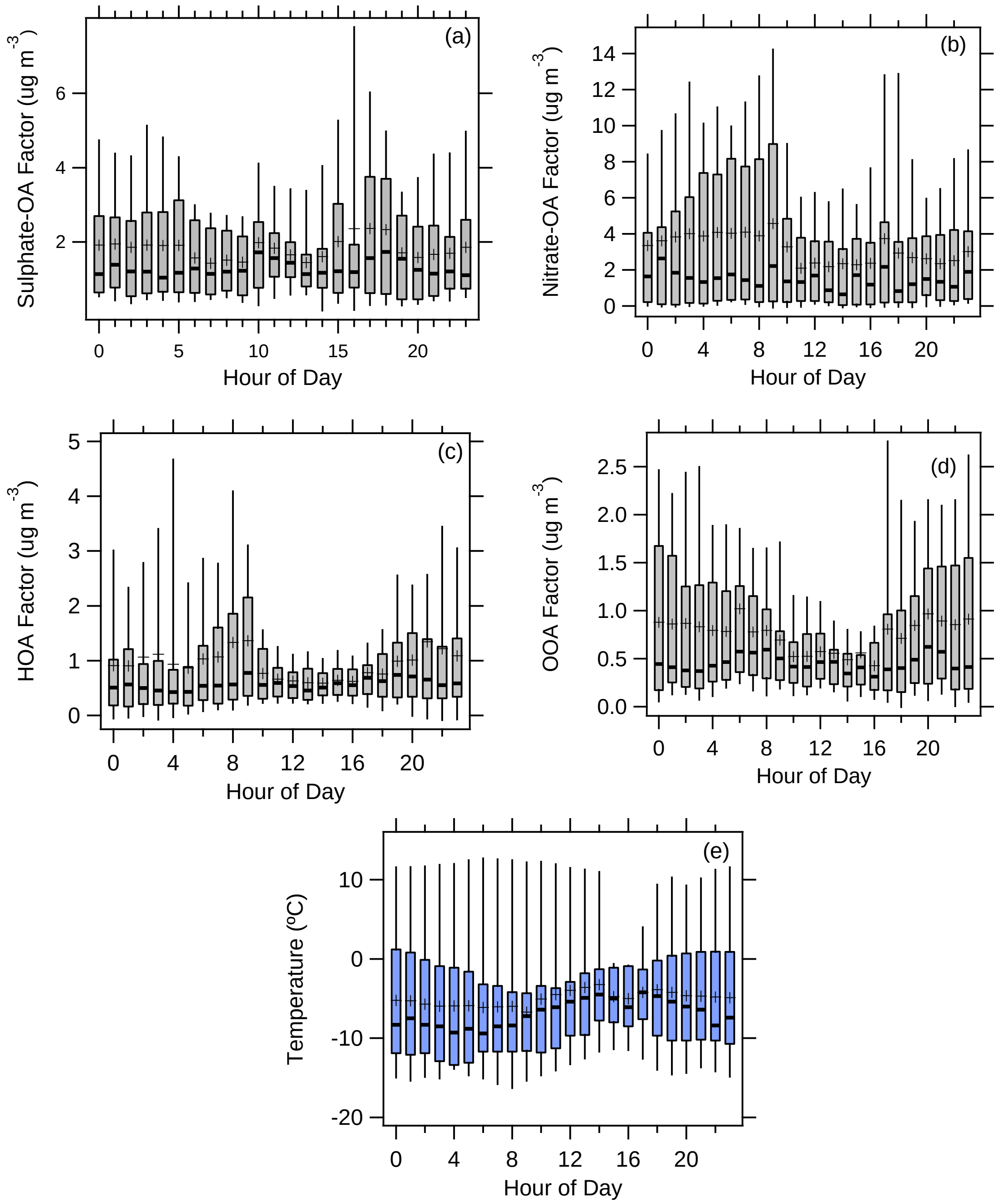

Figure 11: Boxplots of diurnal trends for the Sulphate-OA (a), Nitrate-OA (b), HOA (c), and OOA factors (d), from the PMF$_{\text{Full MS}}$ analysis, along with temperature (e). Boxes indicate interquartile ranges, horizontal lines indicate median hourly values, cross markers indicate hourly means, and whiskers represent the 5th and 95th percentiles. The HOA factor demonstrated a strong diurnal trend consistent with traffic patterns, while the OOA factor demonstrated a trend more consistent with daytime lows and overnight highs. The Nitrate-OA factor showed a minor diurnal trend indicative of more regional contributions as compared to OOA, while the Sulphate-OA factor showed minimal diurnal trend.

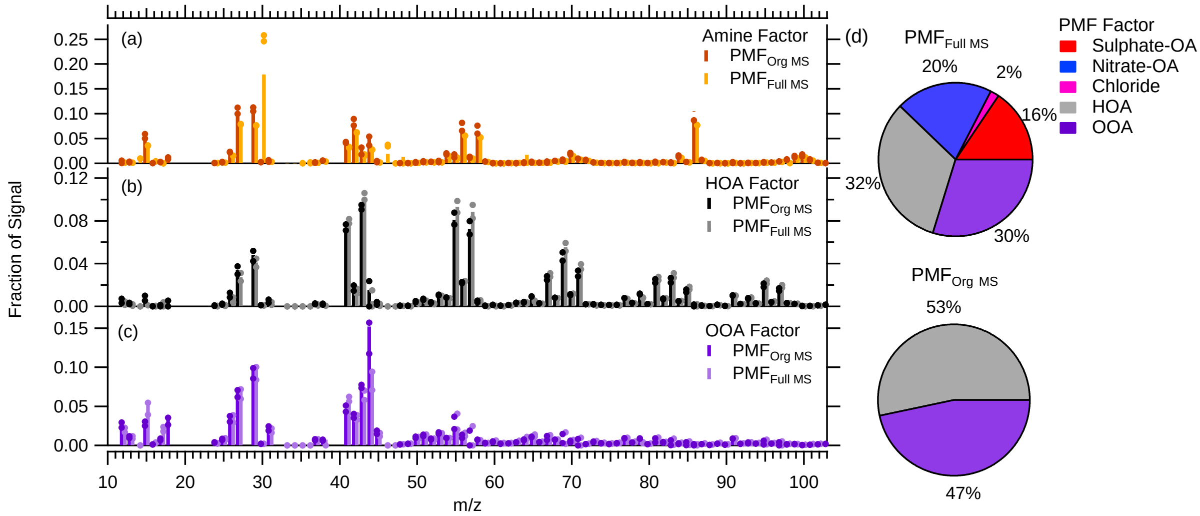

Figure 12: Comparison of factor profiles from the $PMF_{Org\ MS}$ analysis to comparable factors found by PMF of the full mass spectra (a, b, and c). The factors are normalized to the total organic fraction signal, except for the Amine factor which is normalized to the total factor signal. Only minor differences in mass spectra are noted for the HOA factor. The most significant difference for the Amine factor is represented by the addition of the *m/z* 30 peak, and for the OOA factor with the difference in magnitude of the *m/z* 44 peak. Dots show the range in mass spectral variation from FPeak rotations (-10 and 10). Also shown in (d) is the average factor composition of organics for both the PMF of the full mass spectrum and of the organics only.

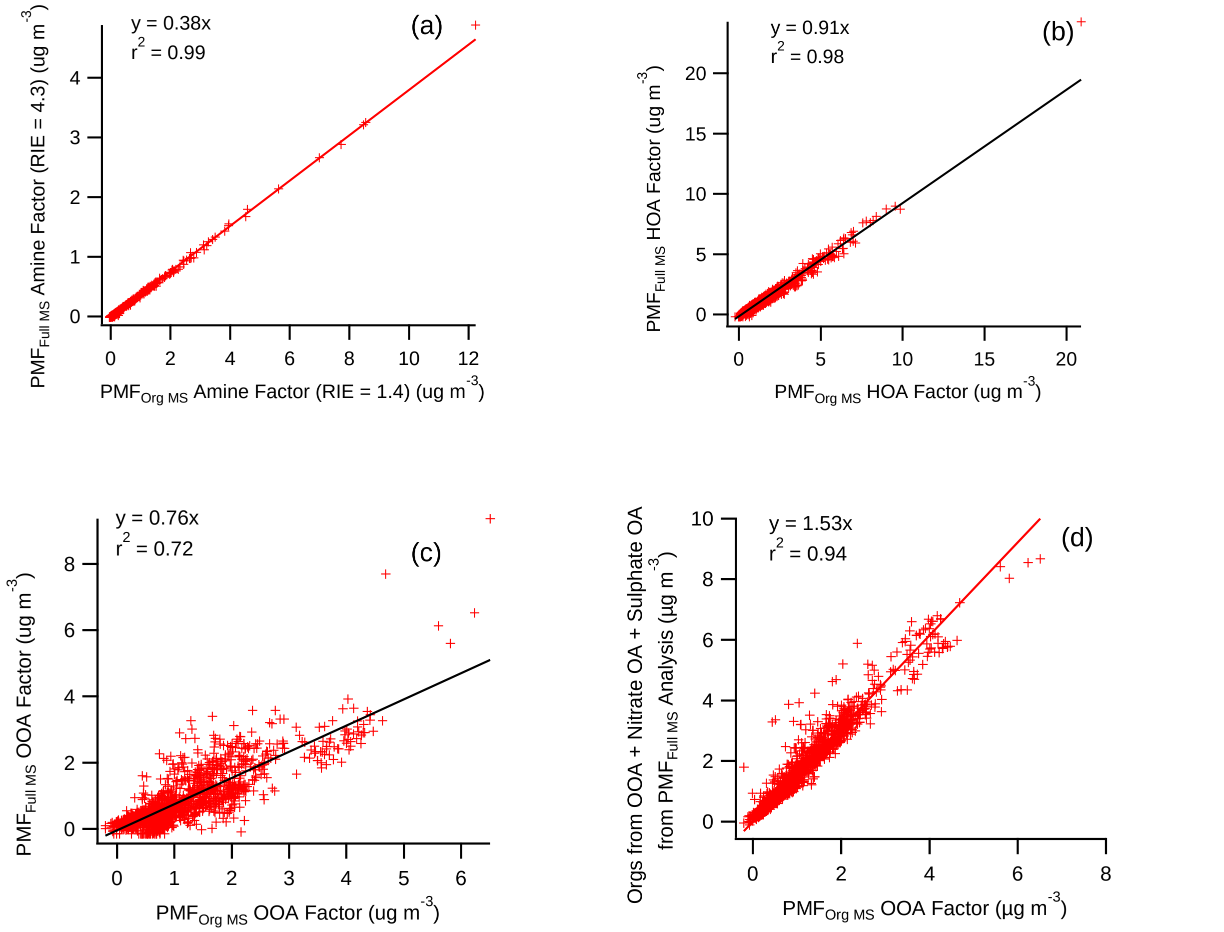

Figure 13: Scatter plots Amine (a), HOA (b), and OOA (c and d) factors comparing their mass derived from $PMF_{Full\ MS}$ vs. $PMF_{Org\ MS}$ analyses. One observation (01/31/2005 21:00) was removed from the HOA comparison to enhance the fit of the trendline.